THE ASTROPHYSICAL JOURNAL, 286:644–658, 1984 November 15

ACCRETING WHITE DWARF MODELS FOR TYPE I SUPERNOVAE. III. CARBON DEFLAGRATION SUPERNOVAE[1]

KEN'ICHI NOMOTO,[2,3,4] FRIEDRICH-K. THIELEMANN,[4] AND KOICHI YOKOI[5]

Received 1984 March 21; accepted 1984 June 1

ABSTRACT

The carbon deflagration models in accreting C+O white dwarfs are presented as a plausible model for Type I supernovae. The evolution of the white dwarf is calculated from the beginning of accretion. The relatively rapid accretion studied here ($\dot{M} \gtrsim 4 \times 10^{-8}\ M_\odot\ \mathrm{yr}^{-1}$) leads to the initiation of the carbon deflagration at the center. Subsequent propagation of the convective carbon deflagration wave and associated explosive nucleosynthesis are calculated for several cases of mixing length in the convection theory. The deflagration wave synthesizes 0.5–0.6 $M_\odot$ ^{56}Ni in the inner layer of the star; this amount is sufficient to power the light curve of Type I supernovae by the radioactive decays of ^{56}Ni and ^{56}Co. In the outer layers, substantial amount of intermediate mass elements, Ca, Ar, S, Si, Mg, and O are synthesized in the decaying deflagration wave; this is consistent with the spectra of Type I supernovae near maximum light. As a result of large nuclear energy release, the star is disrupted completely, leaving no compact star remnant behind. Thus the carbon deflagration model can account for many of the observed features of Type I supernovae.

Nucleosynthesis in the deflagration models is discussed based on the reaction network calculation including 205 species: The abundance ratios of these species with respect to ^{56}Fe normalized to the solar values are shown. These ratios are ~ 1 for ^{40}Ca and ~ 0.5 for ^{36}Ar, ^{32}S, and ^{28}Si. This suggests that Type I supernovae produce a significant fraction of these elements in the Galaxy besides iron peak elements, which may be complementary to the nucleosynthesis in massive star models for Type II supernovae. The production of neutron-rich isotopes, γ-radioactivities, and *s*- and *r*-process elements are discussed.

Finally, the light curves and early time spectra based on the present models are compared with Type I supernova observations.

Subject headings: nucleosynthesis — stars: abundances — stars: accretion — stars: interiors — stars: supernovae — stars: white dwarfs

I. INTRODUCTION

a) *Basic Requirements for Type I Supernova Models*

Type I supernovae (SN I) are quite distinct from Type II supernovae (SN II) because of hydrogen deficiency in their spectra near maximum light. SN I are observed in all types of galaxies including elliptical galaxies and not concentrated in spiral arms (see, e.g., Trimble 1982 and Wheeler 1982 for reviews). These facts can be naturally accounted for by the white dwarf model of SN I. Although this model is currently most popular, whether it is consistent with other observational constraints needs more investigation.

A recent breakthrough in understanding SN I has been brought about by the success of the radioactive decay model (^{56}Ni→ ^{56}Co→ ^{56}Fe) in reproducing the characteristic SN I light curves (Arnett 1979; Colgate, Petsheck, and Kriese 1980; Chevalier 1981; Axelrod 1980*b*; Weaver, Axelrod, and Woosley 1980; Schurmann 1983; Sutherland and Wheeler 1984). This model is supported by the identification of the features in the late time spectra of SN 1972e with emission lines of Fe (Meyerott 1980; Axelrod 1980*a*, *b*) and decaying Co (Axelrod 1980*a*, *b*). The amount of ^{56}Ni required to power the maximum light is estimated to be 0.2–1 $M_\odot$ depending on the Hubble constant (see Wheeler 1982 for a review).

The first hundred days' spectra of SN I 1981*b* have been compared with synthetic spectra (Branch *et al.* 1982, 1983); the maximum-light spectrum is well interpreted by the presence of Ca, Si, S, Mg, O, and possibly Co in the outer layer of SN I at the expansion velocity of $v_{\mathrm{exp}} \approx 10^4$ km s^{-1}.

These results suggest the following composition structure of SN I; the inner layer, exposed at later times, contains 0.2–1 $M_\odot$ ^{56}Ni, while the outer layer, observed at maximum light, is composed mainly of intermediate mass elements Ca-Si-O. The explosion energy is $\sim 10^{51}$ ergs. This picture is consistent with the composition structure of the remnant of SN 1006 suggested from the *IUE* observation by Wu *et al.* (1983). X-ray emission from the Tycho and Kepler supernova remnants also indicates the existence of Si- and S-rich outer shells (Becker *et al.* 1980), although the observation of little enhancement of the iron abundance remains a problem (e.g., Shull 1982).

Thus the present task of the SN I modeling is to calculate detailed nucleosynthesis during explosion and compare it with the suggested composition structure. Such a modeling enables us to calculate a synthetic spectra and see if it is consistent with the observed spectra of SN I.

b) *Detonating White Dwarf Models*

The most plausible model for SN I which is consistent with many of the above features is the thermonuclear explosion of accreting white dwarfs (Hansen and Wheeler 1969; Nomoto 1980*a*, *b*, 1981; Woosley, Weaver, and Taam 1980).

[1] Supported in part by the National Science Foundation grant AST81-15325.
[2] Department of Earth Science and Astronomy, College of Arts and Sciences, University of Tokyo.
[3] Department of Astronomy, University of Illinois.
[4] Max-Planck-Institut für Physik und Astrophysik, Institut für Astrophysik.
[5] Kernforschungszentrum Karlsruhe GmbH, Institut für Kernphysik III.

In earlier papers (Nomoto 1982*a*, *b*, hereafter Paper I and Paper II, respectively), several models of exploding carbon + oxygen (C + O) white dwarfs have been studied from the beginning of accretion of helium through explosion. The evolution during accretion and the supernova models were found to depend on the accretion rate of helium, $\dot{M}$, and the initial mass of the white dwarf, M_{C+O}. Figure 1 shows such a dependence in the parameter space (M_{C+O}, $\dot{M}$), which is an update of Figure 8 in Paper I.

For the accretion as rapid as $\dot{M} \gtrsim 4 \times 10^{-8}\ M_\odot\ \mathrm{yr}^{-1}$, both hydrogen and helium shell flashes are relatively weak and thus increase the C + O core mass (Taam 1980; Fujimoto and Sugimoto 1982). Eventually carbon will be ignited at the center, which triggers a carbon deflagration supernova (Nomoto, Sugimoto, and Neo 1976).

In Papers I and II, cases with relatively slow accretion were investigated. For $4 \times 10^{-8} > \dot{M}\ (M_\odot\ \mathrm{yr}^{-1}) \gtrsim 1 \times 10^{-9}$, the helium shell flash ignited at or near the bottom of accreted helium layer is so strong as to form *double detonation waves*, namely, a helium detonation wave that propagates outward and a carbon detonation wave that propagates inward. The double detonation waves incinerate most of the white dwarf material into ^{56}Ni and the star is disrupted completely.

For still slower accretion with $\dot{M} < 1 \times 10^{-9}\ M_\odot\ \mathrm{yr}^{-1}$, only a *single detonation wave* of helium is formed for $M_{C+O} < 1.1\ M_\odot$ (Paper II; Woosley, Axelrod, and Weaver 1984). If M_{C+O} is larger than $\sim 1.1\ M_\odot$, the central density of the white dwarf reaches the carbon ignition density of $\sim 4 \times 10^9$ g cm^{-3} prior to the helium ignition. Therefore a carbon deflagration supernova will result.

The single detonation processes the accreted helium mostly into ^{56}Ni while the C + O core remains unburned. Such unburned C + O core is either ejected into space or left behind as a white dwarf remnant depending on ($\dot{M}$, M_{C+O}) as shown in Figure 1. The domain in the ($\dot{M}$, M_{C+O}) where the white dwarf remnant is left (Paper II) would be slightly larger than in Figure 1 owing to the hydrodynamical effects (Woosley, Axelrod, and Weaver 1984).

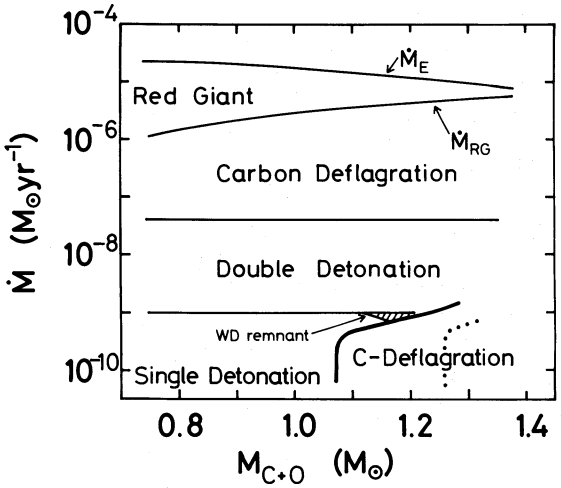

FIG. 1.—Possible models of SN I in C + O white dwarfs, which depend on the accretion rate of helium, $\dot{M}$, and the initial mass, M_{CO}. $\dot{M}_E$ is the Eddington's critical rate for helium. The rapid accretion ($\dot{M} > \dot{M}_{RG}$) forms a red giant–like envelope. For $\dot{M} < 10^{-9}\ M_\odot\ \mathrm{yr}^{-1}$, both single detonation and carbon deflagration are possible depending on M_{CO}, where the solid and dotted lines correspond to the carbon ignition density of 3.5×10^9 and 1×10^{10} g cm^{-3}, respectively. The single detonation results in either the total disruption or explosion leaving a white dwarf remnant (*shaded region*).

In view of nucleosynthesis, the important conclusion of these calculations is that the detonation-type models do not synthesize appreciable amounts of intermediate mass elements, Ca, Ar, S, Si, and O. Therefore the detonating white dwarf models cannot account for the existence of Ca-Si in the outer layers at $v_{exp} \approx 10^4$ km s^{-1}.

The helium detonation models in accreting helium white dwarfs also eject mostly ^{56}Ni (Nomoto and Sugimoto 1977) and thus have the same difficulty in modeling SN I.

c) *Carbon Deflagration Models and Present Study*

In contrast to the inability of the detonation models to account for the early time spectra of SN I, it has been suggested that carbon deflagration models can naturally account for the existence of the outer layers containing Ca-O (Nomoto, Sugimoto, and Neo 1976; Nomoto 1980*a*, *b*, 1981, 1982*c*; Chevalier 1981).

The idea that SN I are triggered by explosive carbon burning in degenerate cores was first presented by Hoyle and Fowler (1960). This idea was developed into the *carbon detonation supernova* model (Arnett 1969) and later into the *carbon deflagration supernova* model as first demonstrated and named by Nomoto, Sugimoto, and Neo (1976). Propagation of a *convective* deflagration wave was calculated by Buchler and Mazurek (1975) only through a relatively early stage and by Nomoto, Sugimoto, and Neo (1976) through explosion of the star. In the models by Ivanova, Imshennik, and Chechetkin (1974), convection was neglected. (See Nomoto 1981; Müller and Arnett 1982, 1984; and Sutherland and Wheeler 1984 for recent models.)

However, only preliminary calculations have been made for nucleosynthesis in the above models so that we need more detailed calculations in order to compare the resultant composition structure with the observations of SN I.

In the present study, therefore, we carried out a detailed nucleosynthesis calculation for the carbon deflagration models of accreting white dwarfs using a reaction network with 205 species. We assumed relatively rapid accretion onto C + O white dwarfs with $\dot{M} \gtrsim 4 \times 10^{-8}\ M_\odot\ \mathrm{yr}^{-1}$ and calculated the evolution from the beginning of accretion through explosion. We have found that these detailed models of deflagration are quite consistent with many of the observed features of SN I. Moreover, the carbon deflagration supernova ejects a substantial amount of intermediate mass elements Ca-Si which are noticeably underproduced relative to the solar abundances in the massive star models for SN II (Woosley and Weaver 1982). The preliminary results have been reported in reviews by Nomoto (1984*b*, *c*; see also Woosley, Axelrod, and Weaver 1984).

In the next section, the input physics is described. In § III, the evolution of the white dwarfs during accretion through the carbon ignition is described. The propagation of the carbon deflagration wave and the hydrodynamic behavior of the exploding white dwarfs are discussed in § IV. Nucleosynthesis in the deflagration wave, the abundances in the ejected matter, and the contribution of SN I to galactic nucleosynthesis are discussed in §§ V–VII, respectively. Comparison with the SN I observations is made in § VIII. Finally, discussions are given in § IX.

II. PHYSICAL INPUT

The implicit hydrodynamic code (Nomoto and Sugimoto 1977; Sugimoto, Nomoto, and Eriguchi 1982) and input

physics are mostly the same as used in Papers I and II except for the following.

Physics for the white dwarf interior includes recent developments in the theory of strongly coupled plasmas (Ichimaru 1982): the equation of state (Slattery, Doolen, and DeWitt 1982), the strong screening factor for nuclear reactions (Ichimaru and Utsumi 1983, 1984), thermal conductivity (Itoh *et al.* 1983), and neutrino-pair bremsstrahlung rate (Itoh and Kohyama 1983). Urca processes (e.g., Iben 1982) were neglected.

Explosive nuclear burning in the deflagration wave was calculated as follows: In the interior with the initial density as high as $\rho_0 > 1 \times 10^8$ g cm^{-3}, a network calculation was carried out until $T \approx 5 \times 10^9$ K using an α-network which includes 14 species (He-Zn). For $T > 5 \times 10^9$ K, the time scale of temperature rise is so short that the incineration of the material into *nuclear statistical equilibrium* (NSE) was assumed. The NSE composition has been tabulated as a function of (ρ, T, Y_e) by Yokoi (update of Yokoi, Neo, and Nomoto 1979; see Thielemann, Nomoto, and Yokoi 1984 for details). Electron captures on the NSE elements were calculated by applying Fuller, Fowler, and Newman's rates (1982). For the outer layers with lower initial density, i.e., $\rho_0 \lesssim 10^8$ g cm^{-3}, the network calculation was carried out until freezing of the reactions.

After the hydrodynamical model was obtained, detailed nucleosynthesis was calculated for all zones behind the deflagration wave using a large network with 205 species (Thielemann, Nomoto, and Yokoi 1984). The energy generation rate and the bulk of the composition based on the large and small networks were found to be consistent.

The nuclear reaction rates were, whenever possible, taken from Fowler, Caughlan, and Zimmerman (1975) including the update by Fowler (1981). For heavier nuclei involving a higher density of compound nuclear resonances, the statistical model calculations from Woosley *et al.* (1975, 1978) were included and complemented in some cases by results obtained with the statistical model code SMOKER (Thielemann 1980). The proton capture rates on proton-rich nuclei by Wallace and Woosley (1981) and, if necessary, the rough estimates of Wagoner, Fowler, and Hoyle (1967) and Wagoner (1969) were taken into account. Weak interaction rates applied in the large network were those from Fuller, Fowler, and Newman (1980, 1982).

III. EVOLUTION OF WHITE DWARFS DURING ACCRETION

a) Models

Two initial models were chosen; one is a C+O core of asymptotic giant branch (AGB) star, and the other is a white dwarf which has been cooled down for 5.8×10^8 yr. Compositions were assumed to be $X(^{12}\mathrm{C}) = 0.475$, $X(^{16}\mathrm{O}) = 0.5$, and $X(^{22}\mathrm{Ne}) = 0.025$. The initial mass is 1.0 $M_\odot$ for both cases, and the initial values of central temperature, T_c, and density, ρ_c, are summarized in Table 1.

The accretion rates were assumed to be $\dot{M} = \dot{M}_{\rm AGB} = 8.5 \times 10^{-7}\ (M/M_\odot - 0.52)\ M_\odot$ yr^{-1} for the core and $\dot{M} = 1 \times 10^{-7}$ and $4 \times 10^{-8}\ M_\odot$ yr^{-1} for the white dwarf. (Hereafter M denotes the mass of the core or white dwarf.) As discussed in Paper I, the accretion of hydrogen-rich matter at a rate of $\dot{M}_{\rm AGB} \gtrsim \dot{M} \gtrsim 4 \times 10^{-8}\ M_\odot$ yr^{-1} results in a steady or weakly unstable hydrogen shell burning. Accretion of helium with $\dot{M} \gtrsim 4 \times 10^{-8}\ M_\odot$ yr^{-1} also leads to a weak flash. Therefore the accretion increases the mass of the C+O white dwarf through recurrence of the shell flashes. We approximated such an increase in M by assuming the steady hydrogen-helium shell burning where the accreted material is processed into C+O at the same rate as the accretion. The hydrogen shell burning was treated by the thin-shell approximation (Hayashi, Hōshi, and Sugimoto 1962), and the mass of the helium layer is determined by the steady state condition. The temperature at the helium burning shell, which is higher for higher $\dot{M}$, is roughly 1.5×10^8 K for the present $\dot{M}$.

The case with $\dot{M} = 1 \times 10^{-9}\ M_\odot$ yr^{-1} was also calculated with the same approximation as above in order to see the effects of accretion rate on the evolution.

TABLE 1

INITIAL AND IGNITION MODELS

	Initial Models[a]		Ignition Models		
Model	ρ_c (g cm^{-3})	T_c (K)	ρ_c (g cm^{-3})	$M/M_\odot$	$E_{\rm Bind}$ (ergs)
Core	2.9×10^7	1×10^8	1.5×10^9	1.366	5.0×10^{51}
WD[b]	3.4×10^7	1×10^7	2.6×10^9	1.378	5.3×10^{51}

[a] $M = 1.0\ M_\odot$.

[b] The accreting white dwarf with $\dot{M} = 4 \times 10^{-8}\ M_\odot$ yr^{-1}.

b) Heating of the White Dwarf

Figure 2*a* shows the temperature, T, and density, ρ, plane. A change in the ρ-T structure line of the white dwarf during the accretion for $\dot{M} = 4 \times 10^{-8}\ M_\odot$ yr^{-1} is shown by the dashed lines, and the evolutionary tracks corresponding to the central conditions, i.e., (ρ_c, T_c) for both the core and the white dwarf, are shown by the solid lines. (Hereafter the subscript c denotes the center.)

As matter is accreted, both ρ_c and T_c increase by compression. At the same time, heat flows from the outer hot layer into the central cold layer by conduction. Since the time scale of heat conduction is $\sim 2 \times 10^6$ yr, central entropy starts to increase at $t_{\rm acc} \approx 2 \times 10^6$ yr, where $t_{\rm acc}$ is the time measured from the beginning of accretion. In the present models, there exist two heating sources: One is the hydrogen-helium double shell-burning, and the other is the rapid compression of the outer layer by accretion (see eq. [8] in Paper I). These two effects are comparable for $\dot{M} \gtrsim 4 \times 10^{-8}\ M_\odot$ yr^{-1}.

As a result, T_c increases to reach $\sim 10^8$ K where the neutrino loss determines the thermal structure; i.e., entropy starts to decrease in the central region and, because of the density dependence of the neutrino loss rate, the temperature inversion disappears near the center. Afterwards the evolution of (ρ_c, T_c) is controlled by the balance between the compressional heating and neutrino loss, which depends only on $\dot{M}$ (Sugimoto and Nomoto 1980, p. 178).

For $\dot{M} = 1 \times 10^{-7}$ and $1 \times 10^{-9}\ M_\odot$ yr^{-1}, the evolutionary tracks of (ρ_c, T_c) are shown in Figure 2*b*. For the case with faster accretion, substantial heating of the core commences at the stage with higher ρ_c (or larger M) since the heat conduction time scale is $\sim 2 \times 10^6$ yr (Fig. 2*b*). The central temperature reaches the common evolutionary track, which is determined only by $\dot{M}$, at $\rho_c \approx 1 \times 10^9$ and 4×10^7 g cm^{-3} for $\dot{M} = 1 \times 10^{-7}$ and $1 \times 10^{-9}\ M_\odot$ yr^{-1}, respectively.

If the initial mass of the white dwarf is larger than, say, 1.2 $M_\odot$, or $\dot{M}$ is higher, $t_{\rm acc}$ would be shorter than $\sim 2 \times 10^6$ yr at the carbon ignition, i.e., there would be not enough time for the

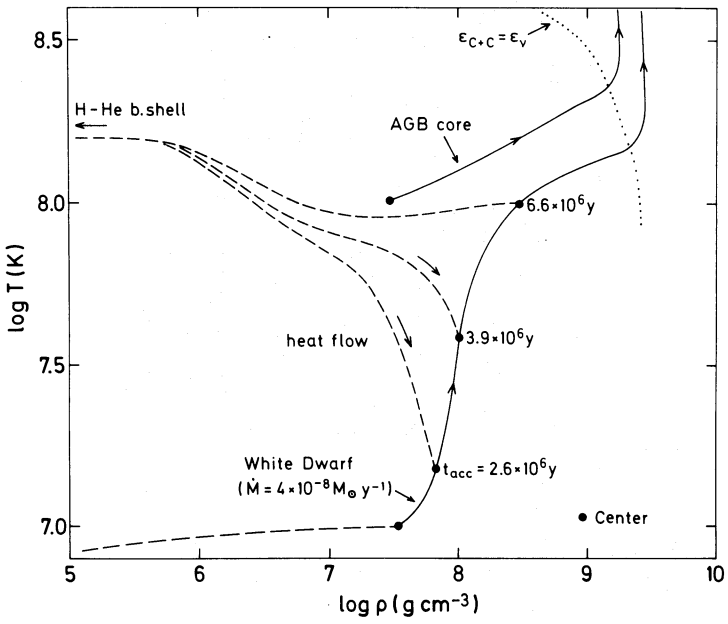

FIG. 2a

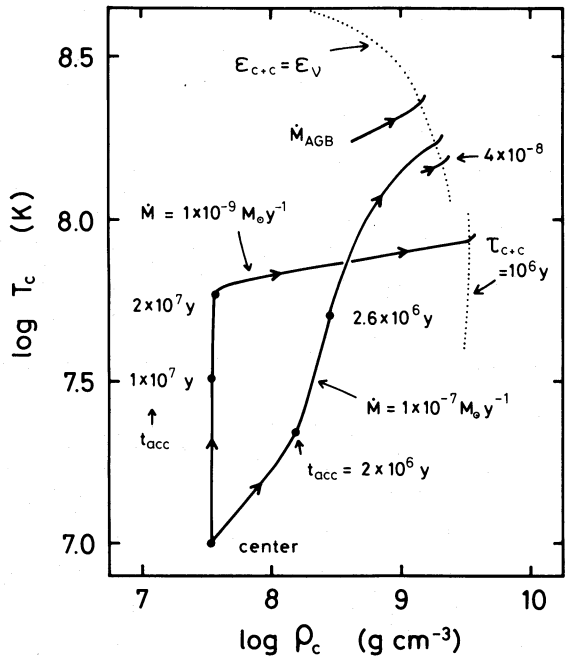

FIG. 2b

FIG. 2—(*a*) Accretion onto the white dwarf ($\dot{M} = 4 \times 10^{-8}\ M_\odot\ \mathrm{yr}^{-1}$) and growth of the core in the AGB star. The evolution of (ρ_c, T_c) is shown by the solid lines. Time, t_{acc}, is measured from the onset of accretion. Dashed lines are the structure lines of the white dwarf where heat flows from the surface into the interior. The dotted line is the ignition line of carbon burning defined by $\epsilon_{C+C} = \epsilon_\nu$. (*b*) Same as Fig. 2*a* but for the accretion onto the white dwarf with $\dot{M} = 1 \times 10^{-7}$ and $1 \times 10^{-9}\ M_\odot\ \mathrm{yr}^{-1}$. For low temperature, the carbon ignition occurs approximately at $\tau_{C+O} \equiv c_p T/\epsilon_{C+C} = 10^6$ yr as indicated by the dotted line.

substantial heat inflow into the central region before the carbon ignition point is reached. In other words, the ignition density would depend on the initial condition of the white dwarf. Such a situation is actually seen in the models with $\dot{M} > \dot{M}_{AGB}$ (Nomoto 1984*c*).

Similar results were obtained in a preliminary calculation for the colder white dwarf with a crystallized central region. The white dwarf is first melted by heat inflow from the surface layer and the evolution of (ρ_c, T_c) merges into the same track as determined only by $\dot{M}$ in Figure 2*a*.

c) *Carbon Ignition*

When the evolutionary path of (ρ_c, T_c) reaches the dotted line in Figures 2*a*–2*b* which corresponds to $\epsilon_{C+C} = \epsilon_\nu$ for higher temperature and $\tau_{C+C} \equiv c_p T/\epsilon_{C+C} \approx 10^6$ yr for low temperature, carbon is ignited at the center. Here ϵ_{C+C} and ϵ_ν denote the nuclear energy generation rate and the neutrino loss rate, respectively, and c_p is the specific heat. Because of strong electron degeneracy, carbon burning is unstable to a flash, and T_c increases rapidly as seen in Figure 2*a*.

The central density, $\rho_{c,ig}$, and the mass of the white dwarf at the carbon ignition, summarized in Table 1 for the core and the white dwarf with $\dot{M} = 4 \times 10^{-8}\ M_\odot\ \mathrm{yr}^{-1}$, are important quantities for the subsequent evolution and nucleosynthesis. For larger $\dot{M}$, faster compression ignites the carbon at higher T_c and lower ρ_c. For smaller $\dot{M}$, on the other hand, T_c is lower and thus $\rho_{c,ig}$ is higher (Fig. 2*b*; also Ergma and Tutukov 1976).

It should be noted, however, that extremely rapid accretion such as $\dot{M} > \dot{M}_{AGB}$ compresses the central region almost adiabatically; therefore, $\rho_{c,ig}$ depends mainly on central entropy and thus is higher for the initially colder white dwarf (Nomoto 1984*c*).

IV. HYDRODYNAMIC BEHAVIOR OF CARBON DEFLAGRATION SUPERNOVAE

a) *Formation of a Carbon Deflagration Wave*

The central carbon flash grows into thermonuclear runaway because of strong electron degeneracy. The so-called convective Urca processes, which were ignored in the present calculation, would delay the occurrence of the runaway until ρ_c reaches $\sim 1.5 \times \rho_{c,ig}$ (Iben 1982). The subsequent hydrodynamic phases were calculated for two cases, i.e., the C+O core and the white dwarf with $\dot{M} = 4 \times 10^{-8}\ M_\odot\ \mathrm{yr}^{-1}$. The development of the thermonuclear runaway to form a deflagration or detonation wave is as follows, which is discussed in detail in § II of Paper II: When the central temperature, T_c, reaches $\sim 8 \times 10^8$ K, convection can no longer transport the released energy so that the blocking of heat occurs in the central region. Soon T_c exceeds T_{def} (Paper II), i.e., the time scale of temperature rise exceeds the dynamical time scale. Afterwards the material is incinerated into NSE composition.

The released nuclear energy, $q \sim 3 \times 10^{17}$ ergs g^{-1}, is only 20% of the internal energy of degenerate electrons, u_0 (see Fig. 2 of Paper II), so that the thermal overpressure is too small to ignite carbon in the adjacent layer. In other words, a carbon detonation wave does not form (cf. Ivanova, Imshennik, and Chechetkin 1974; Buchler and Mazurek 1975; Nomoto, Sugimoto, and Neo 1976; Mazurek, Meier, and Wheeler 1977). To initiate the Chapman-Jouguet detonation, $q \approx u_0$ is required according to the shock-tube analysis (Mazurek, Meier, and Wheeler 1977). Moreover, the spherical geometry in the central region significantly damps the shock wave (Ōno 1960), so that larger q/u_0 is required. It should be noted that the carbon detonation models (Arnett 1969; Bruenn 1971) *assumed* the formation of a detonation wave.

b) Propagation of the Carbon Deflagration Wave

After the thermonuclear runaway in the central region, the explosive carbon burning front propagates outward on the time scale for convective energy transport across the front, because the density inversion at the front is unstable to Rayleigh-Taylor instability (see the 2D calculation by Müller and Arnett 1982, 1984 for the development of Rayleigh-Taylor instability). A burning front which propagates at a subsonic velocity with respect to the unburned material is called a deflagration wave in contrast to a detonation wave which propagates at a supersonic velocity (e.g., Courant and Friedrichs 1948).

To simulate the propagation of a convective carbon deflagration wave with a 1D hydrodynamic code, the time-dependent mixing-length theory of convection by Unno (1967) was employed. The mixing length, l, was taken to be $l = \alpha H_p$, where H_p is a pressure scale height and α is a parameter.

Two cases with $\alpha = l/H_p = 0.6$ (case C6) and 0.8 (C8) for the core and three cases with $\alpha = 0.6$ (W6), 0.7 (W7), 0.8 (W8) for the white dwarf were calculated. Here the results for case W7 will be discussed in detail. Figure 3 shows the propagation of the deflagration wave and the associated expansion of the Lagrangian shells. Changes in the profiles of temperature, density, and velocity are shown in Figures 4*a*–4*c*, where the time corresponding to the stage number is given in the legend.

The propagation velocity, v_{DF}, of the deflagration wave with respect to the unburned material is slow in the early stages; e.g., $v_{DF} \approx 0.08 v_s$ for stage 2, where v_s is the sound velocity of the burned material. As the deflagration wave propagates outward, v_{DF} gets larger because of the increasing density jump across the front. However, at stage 7, v_{DF} is still as slow as $\sim 0.3 v_s$. Thus it takes 1.2 s for the deflagration wave to reach the shell at $M_r = 1.3\ M_\odot$ (Fig. 3) which is 6 times longer than the propagation of a detonation wave (Arnett 1969).

During the slow propagation of the deflagration wave, the white dwarf gradually expands (Fig. 3) to decrease the density and temperature (Figs. 4*a*–4*b*). Such an expansion weakens the explosive nuclear burning at the deflagration wave and eventually quenches the carbon burning when the deflagration wave reaches $M_r = 1.3\ M_\odot$ where $\rho \approx 10^7$ g cm^{-3}.

In the present calculation, modeling after the quenching of explosive burning is only approximate. At the location where nuclear burning dies out, the density inversion still exists (stage 9 in Fig. 4*b*) because of such a large temperature jump as 3×10^9 K (Fig. 4*a*). Therefore mixing between the hot and cold matter should occur owing to Rayleigh-Taylor instability, which was not followed in the present calculation (but followed in the models by Nomoto 1980*a*, 1981). Thus abundances of mild carbon burning products, in particular, ^{20}Ne, ^{23}Na, and ^{24}Mg discussed in § IV, should be regarded as approximate by a factor of roughly 2 (Mg, Ne) and more than 10 (Na).

The deflagration wave compresses the material ahead of it and forms a precursor shock wave as seen from the density and velocity profiles (Figs. 4*b*–4*c*). This precursor shock is not so strong as to ignite carbon in most cases; in other words, the deflagration wave does not grow into a detonation. When the deflagration wave arrives at the outer layer around $M_r \approx 1.3\ M_\odot$, however, the precursor shock is strengthened owing to the steep density gradient near the surface. Whether the shock ignites carbon depends on the propagation speed of the deflagration wave and also the preshock temperature. For the present models, carbon ignition in the outer layer does occur for case C8 but does not for other cases.

TABLE 2

ENERGETICS OF EXPLOSION

PARAMETER	CORE CASES		WD CASES		
	C6[a]	C8[b]	W6[c]	W7[d]	W8[e]
E(nuclear)[f]	1.4	1.9	1.5	1.8	2.0
E(neutrino)[f]	0.018	0.020	0.033	0.035	0.037
E(kinetic)[f]	0.91	1.4	0.99	1.3	1.5
$M(^{56}\mathrm{Ni})/M_\odot$	0.48	0.64	0.49	0.58	0.65

[a] $\dot{M} = \dot{M}_{AGB}$; $\alpha = 0.6$.
[b] $\dot{M} = \dot{M}_{AGB}$; $\alpha = 0.8$.
[c] $\dot{M} = 4 \times 10^{-8}\ M_\odot\ \mathrm{yr}^{-1}$; $\alpha = 0.6$.
[d] $\dot{M} = 4 \times 10^{-8}\ M_\odot\ \mathrm{yr}^{-1}$; $\alpha = 0.7$.
[e] $\dot{M} = 4 \times 10^{-8}\ M_\odot\ \mathrm{yr}^{-1}$; $\alpha = 0.8$.
[f] Energies in units of 10^{51} ergs.

c) Energetics of Explosion

The energetics of the deflagration are summarized for several models in Table 2. For the model with faster deflagration, i.e., larger α, more material is processed by the deflagration wave

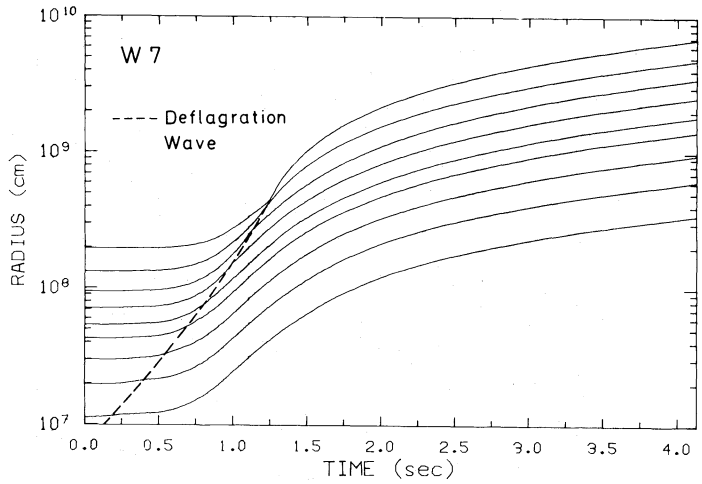

FIG. 3.—Propagation of the carbon deflagration wave (*dashed line*) and the associated expansion of the Lagrangian shells for case W7. Time is measured from the initiation of the deflagration. These shells correspond to $M_r/M_\odot = 0.007, 0.03, 0.10, 0.25, 0.41, 0.70, 1.00, 1.28$, and 1.378 from the interior to the exterior.

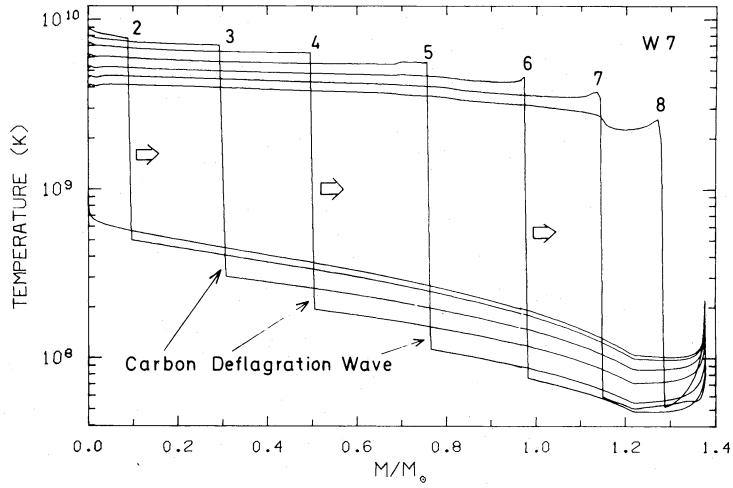

FIG. 4*a*

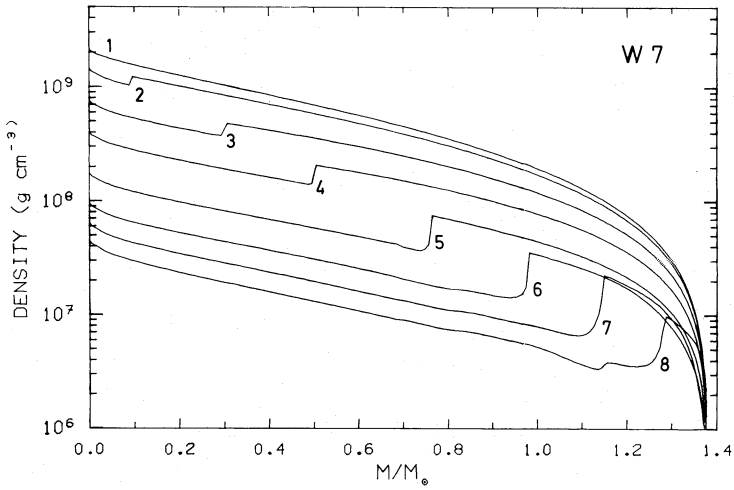

FIG. 4*b*

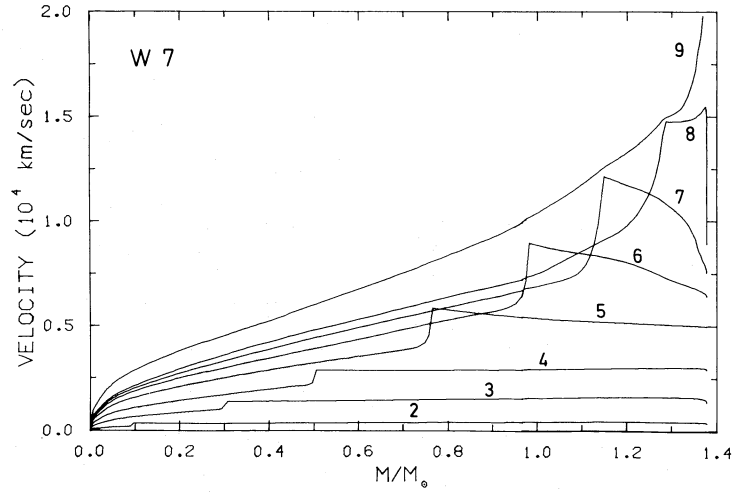

FIG. 4*c*

FIG. 4.—(*a*) Change in the temperature distribution during the propagation of the carbon deflagration wave (case W7). Stage numbers 1–9 correspond to t(s) = 0.0 (1), 0.60 (2), 0.79 (3), 0.91 (4), 1.03 (5), 1.12 (6), 1.18 (7), 1.24 (8), 3.22 (9), respectively, where t is the same as in Fig. 3. (*b*) Same as Fig. 4*a* but for the density distribution. (*c*) Same as Fig. 4*c* but for the velocity distribution.

before quenching, and thus larger nuclear energy, E_n, is released. The dependence of E_n on the ignition density is relatively small within the present parameter range, although E_n is slightly larger for higher $\rho_{c,ig}$. On the other hand, neutrino energy loss, E_ν, depends sensitively on $\rho_{c,ig}$, because electron captures in the central region determine E_ν.

The total nuclear energy release exceeds the initial binding energy of the white dwarf and the core so that the star is disrupted completely leaving no compact star behind. Because of the low $\rho_{c,ig}$, neutrino energy losses associated with electron captures are as small as 10^{49} ergs, and thus negligible. The explosion energy is $\sim 10^{51}$ ergs, which is in good accord with SN I.

As seen from the velocity profile at stage 9 (Fig. 4*c*), the expansion velocity of $v_{exp} = 10{,}000$–$14{,}000$ km s^{-1} deduced from the spectra near maximum light is seen at $M_r = 0.9$–1.2 $M_\odot$ in model W7. For case C6, the same range of v_{exp} appears at $M_r = 1.1$–1.3 $M_\odot$. Therefore, even the weakest explosion among the present models is consistent with the early time observations.

Models with much slower deflagration were calculated by Nomoto, Sugimoto, and Neo (1976) with more simplified treatment of deflagration; it was found that the star once oscillates because of too small nuclear energy release and ultimately explodes with the energy as small as 5×10^{49} ergs.

d) Neutrino Bursts

Behind the deflagration wave, the hot processsed materials undergo electron captures so that the associated neutrinos, mostly ν_e, are emitted from the white dwarf. Figure 5 shows the time profile of the neurino luminosity, L_ν, during the propagation of the deflagration wave for cases W7 and C6. The peak value of L_ν is 7×10^{49} ergs s^{-1} (W7) which is much smaller than that expected from SN II during the core collapse (e.g., Mazurek, Cooperstein, and Kahana 1980). The neutrino luminosity should not be so high because the ejected materials should not be too much neutronized by electron captures (see § VI).

The observation of such a neutrino burst, especially its time profile, could give a useful information on the propagation speed of the deflagration wave which is very uncertain at the present level of convection theory.

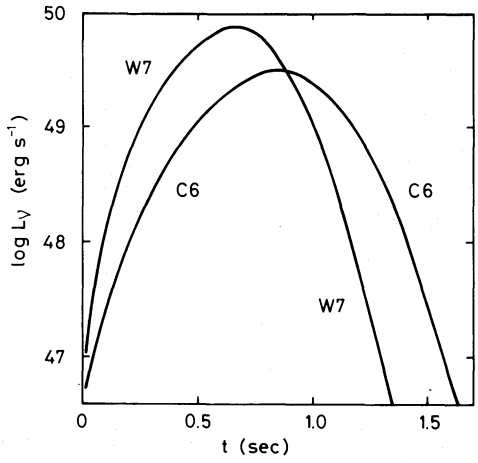

FIG. 5.—Time profile of the neutrino luminosity, L_ν, for cases W7 and C6. Neutrinos are emitted associating with electron captures behind the deflagration wave.

V. EXPLOSIVE NUCLEOSYNTHESIS IN THE CARBON DEFLAGRATION WAVE

The white dwarf material undergoes explosive burning of carbon, neon, oxygen, and silicon at the passage of the deflagration wave in a generalized sense according to final burning products. The nucleosynthesis calculations were carried out until freezing for all zones. Changes in temperature and density for several zones are shown in Figures 6*a*–6*b* against time. The nuclear products of such explosive burning depends mainly on the peak temperature, T_p, and the corresponding density, ρ_p, at the deflagration wave as will be described below. The final composition structure based on the network calculation is shown in Figure 7*a* for W7 and Figure 7*b* for case C6. The main features of nucleosynthesis for case W7 are as follows, and more details will be given elsewhere (Thielemann, Nomoto, and Yokoi 1984).

a) Inner NSE Layer

For the inner layer at $M_r < 0.7$ $M_\odot$, $\rho_{p,7} \gtrsim 9$ and $T_{p,9} \gtrsim 6$ so that the nuclear reactions are rapid enough to incinerate the material into almost NSE composition. Here $\rho_{p,7} \equiv \rho_p/10^7$ g cm^{-3} and $T_{p,9} \equiv T_p/10^9$ K. As the white dwarf expands, the interior temperature decreases as seen in Figure 6*a* and the composition changes into iron peak elements. As seen in Figure 7, the central layers are composed of neutron-rich iron peak elements (^{56}Ni, ^{56}Fe, ^{54}Fe) because of electron captures at the high density; the number of electron per baryon at the center is $Y_e = 0.46$ for case W7 and 0.47 for case C6. (The distribution of Y_e is shown in Fig. 8.) In the lower density region at $M_r \gtrsim 0.1$ $M_\odot$, Y_e is larger so that ^{56}Ni is the dominant product.

It is noteworthy that some intermediate mass elements, ^{40}Ca, ^{36}Ar, and ^{32}S, exist in minor amounts at $0.3 \lesssim M_r/M_\odot \lesssim 0.6$ where iron peak elements are dominant. This indicates that partial breakdown of NSE occurs during the freezing because reactions cannot keep pace with the change in the NSE composition due to the rapid decrease in (ρ, T). (See the difference between the NSE composition [Figs. 6–7 in Nomoto 1984*b*] and Figs. 7*a*–7*b* of the present work.) Further careful study is needed to see how such a partial breakdown of NSE depends on the freeze-out conditions (Thielemann, Nomoto, and Yokoi 1984).

b) Outer Partially Burned Layer

When the deflagration wave reaches the outer layers at $M_r \gtrsim 0.7$ $M_\odot$ ($t \gtrsim 1$ s), the white dwarf has already expanded, and ρ_c has decreased by a factor of more than 10. Therefore the density at the front is significantly lower than the initial value at $t = 0$ as seen in Figure 6*b*.

The peak temperature attained during explosive burning, T_p, is lower for lower density because of larger heat capacity. Moreover, the temperature and density quickly decrease after the passage of the deflagration wave owing to an accompanying rarefaction wave as well as the rapid expansion of the white dwarf (Figs. 6*a*–6*b*). These effects slow down the nuclear reactions so that the material undergoes explosive burning but is not incinerated into NSE composition. The resultant composition structure is also shown in Figures 7*a*–7*b*.

For the layers at $0.7 \lesssim M_r/M_\odot < 0.9$, T_p is as low as $6 > T_{p,9} \gtrsim 5$, and the corresponding density is $9 > \rho_{p,7} \gtrsim 4$. The reactions are not rapid enough to process the material into ^{56}Ni; in other words, this layer undergoes partial Si-burning, whose products are ^{28}Si, ^{32}S, ^{36}Ar, ^{40}Ca, ^{54}Fe, ^{56}Ni, etc.

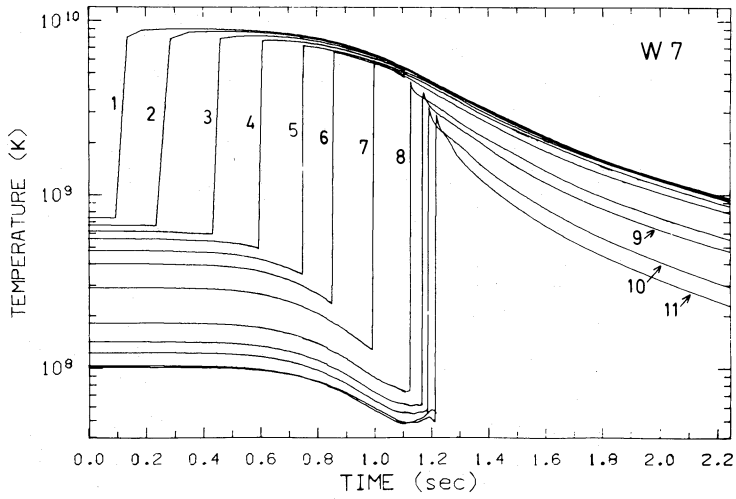

FIG. 6a

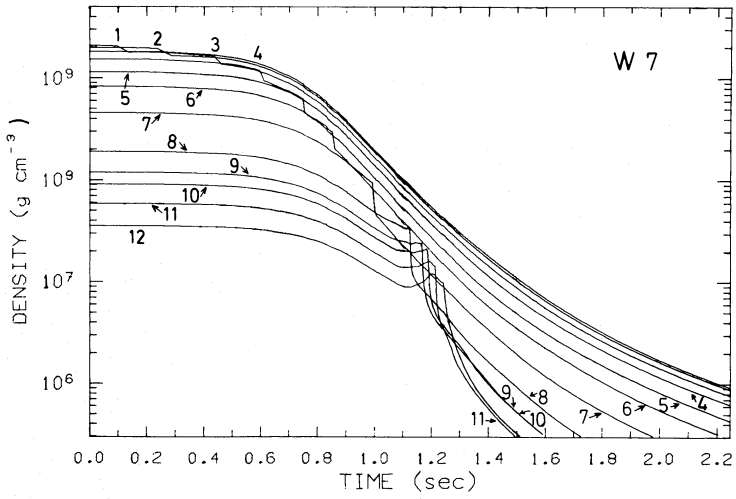

FIG. 6b

FIG. 6.—(*a*) Changes in the temperatures with time for several zones for case W7. At late times, the temperature decreases owing to the expansion of the white dwarf. Zone numbers 1–12 correspond to the Lagrangian shells with $M_r/M_\odot = 0.0011, 0.009, 0.036, 0.10, 0.25, 0.41, 0.70, 1.00, 1.12, 1.17, 1.23$, and 1.29, respectively. (*b*) Same as Fig. 6*a* but for the density.

For $0.9 \lesssim M_r/M_\odot < 1.1$, $5 > T_{p,9} \gtrsim 4$, and $4 > \rho_{p,7} \gtrsim 2.5$. Explosive carbon and oxygen burning produces ^{28}Si, ^{32}S, and ^{36}Ar, but T_p is too low for Si burning to proceed. Thus this layer is rich in Si peak elements.

For $1.1 \lesssim M_r/M_\odot < 1.25$, $4 > T_{p,9} \gtrsim 3$ so that this layer undergoes explosive carbon and neon burning which produces ^{16}O, ^{24}Mg, ^{28}Si, etc. but oxygen burning is too slow to proceed appreciably. Finally, in the quenching phase of the deflagration wave, only the carbon-burning products appear at $1.25 \lesssim M_r/M_\odot < 1.3$. In the outermost layer at $M_r \gtrsim 1.3\ M_\odot$, the original C+O remains unburned. As mentioned in § IV*b*, the compositions around $M_r \approx 1.3\ M_\odot$ are approximate.

c) Dependence on the Propagation Speed of the Deflagration Wave

The mass of produced ^{56}Ni depends on the propagation speed, v_{DF}, of the deflagration wave as summarized in Table 2. For larger $\alpha \equiv l/H_p$, almost complete incineration of the white dwarf material is resulted and the mass of Ca-Si is negligibly small. On the other hand, the model with much slower deflagration by Nomoto, Sugimoto, and Neo (1976) produces only 0.2 $M_\odot$ iron peak elements.

VI. ABUNDANCES IN THE EJECTA

The deflagrating white dwarfs are disrupted completely and all the synthesized elements in Figures 7*a*–7*b* are ejected into space. The integrated mass and the ratio of $\langle X_i/X(^{56}\mathrm{Fe})\rangle \equiv [X_i/X(^{56}\mathrm{Fe})]/[X_i/(^{56}\mathrm{Fe})]_\odot$ for the typical species are summarized in Table 3. The abundances of other stable isotopes are shown in Table 4 and Figure 9 for case W7. Here the solar abundances were taken from Cameron (1982). Case C6 shows an almost identical pattern except for the smaller abundances of neutron-rich species and the larger ^{16}O abundance (Table 5 and Fig. 11). Figures 10 and 12 show the abundances of elements relative to the solar values, which is normalized to Si for cases W7 and C6, respectively.

a) Iron Peak Elements

The mass of the iron peak elements is 0.86 $M_\odot$ (W7) and 0.66 $M_\odot$ (C6). Among them, ^{56}Ni amounts to 0.5–0.6 $M_\odot$ (Table 2)

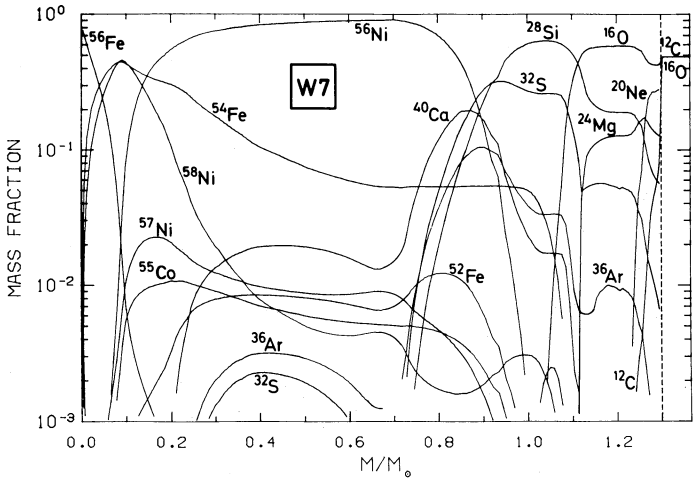

FIG. 7a

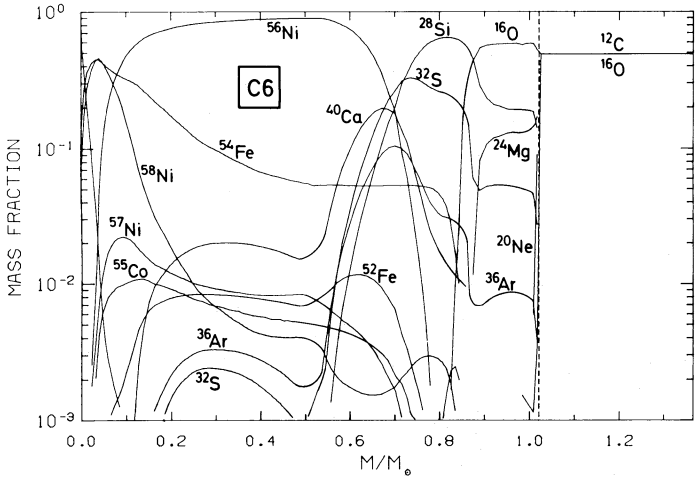

FIG. 7b

FIG. 7.—(*a*) Composition structure in the white dwarf after the freezing of nuclear reactions for case W7. At $M_r < 0.7\ M_\odot$ the white dwarf undergoes incineration into almost NSE composition. In the intermediate region at $0.7 \lesssim M_r/M_\odot < 1.3$, the white dwarf undergoes partial explosive burning. In the outer layer ($M_r \gtrsim 1.3\ M_\odot$), C+O remain unburned. (*b*) Same as Fig. 7*a* but for the case C6.

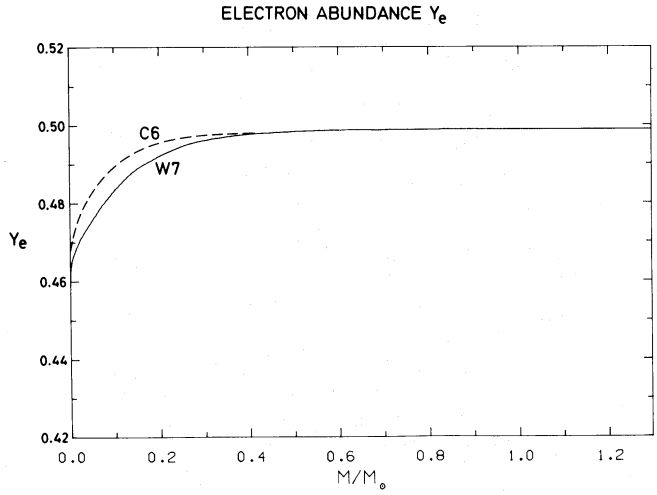

FIG. 8.—Distribution of the number of electrons per baryon, Y_e, for both cases W7 and C6.

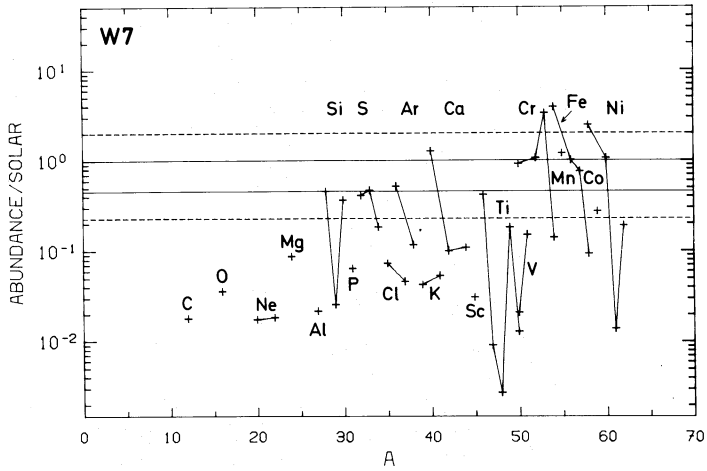

FIG. 9.—Nucleosynthesis in the carbon deflagration model W7. The abundances of stable isotopes relative to the solar values are shown. The ratio is normalized to ^{56}Fe.

TABLE 3

ABUNDANCES OF MAJOR PRODUCTS

	CASE W7		CASE C6	
SPECIES	Mass ($M_\odot$)	$\langle X_i/^{56}\mathrm{Fe}\rangle^a$	Mass ($M_\odot$)	$\langle X_i/^{56}\mathrm{Fe}\rangle^a$
Cr–Ni	0.86	...	0.66	...
^{58}Ni	0.061	2.4	0.040	2.0
^{56}Fe	0.613	1	0.487	1
^{54}Fe	0.145	3.9	0.107	3.6
^{40}Ca	0.041	1.3	0.035	1.4
^{36}Ar	0.022	0.52	0.018	0.54
^{32}S	0.082	0.41	0.068	0.42
^{28}Si	0.155	0.45	0.130	0.48
^{24}Mg	0.023	0.087	0.017	0.081
^{20}Ne	0.011	0.017	0.001	0.002
^{16}O	0.140	0.036	0.255	0.082
^{12}C	0.032	0.018	0.166	0.12

[a] $\langle X_i/^{56}\mathrm{Fe}\rangle \equiv [X_i/X(^{56}\mathrm{Fe})]/[X_i/X(^{56}\mathrm{Fe})]_\odot$.

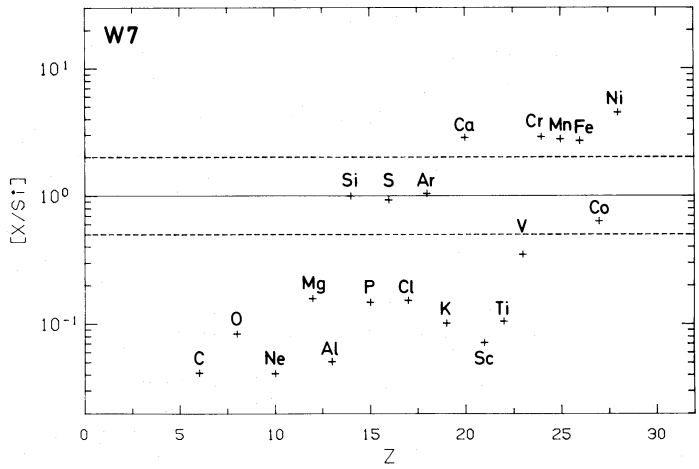

FIG. 10.—The abundances of elements relative to the solar values (W7). The ratio is normalized to Si.

TABLE 4

NUCLEOSYNTHESIS PRODUCTS FOR THE MODEL W7

Species	Mass ($M_\odot$)	$\langle X_i/X_i(^{56}\mathrm{Fe})\rangle$[a]
^{12}C	3.2 E−02	1.8 E−02
^{13}C	7.6 E−13	3.6 E−11
^{14}N	4.8 E−09	1.1 E−08
^{15}N	2.1 E−08	1.3 E−05
^{16}O	1.4 E−01	3.6 E−02
^{17}O	2.9 E−10	1.9 E−07
^{18}O	4.5 E−12	5.0 E−10
^{19}F	2.9 E−11	1.5 E−07
^{20}Ne	1.1 E−02	1.7 E−02
^{21}Ne	4.1 E−08	2.1 E−05
^{22}Ne	1.5 E−03	1.8 E−02
^{23}Na	1.8 E−05	9.9 E−04
^{24}Mg	2.3 E−02	8.7 E−02
^{25}Mg	7.8 E−06	2.2 E−04
^{26}Mg	2.4 E−05	6.0 E−04
^{27}Al	6.6 E−04	2.2 E−02
^{28}Si	1.6 E−01	4.5 E−01
^{29}Si	4.6 E−04	2.6 E−02
^{30}Si	4.5 E−03	3.6 E−01
^{31}P	1.7 E−04	6.4 E−02
^{32}S	8.2 E−02	4.1 E−01
^{33}S	7.8 E−04	4.7 E−01
^{34}S	1.7 E−03	1.8 E−01
^{36}S	2.3 E−08	7.2 E−04
^{35}Cl	1.2 E−04	7.3 E−02
^{37}Cl	2.6 E−05	4.6 E−02
^{36}Ar	2.2 E−02	5.2 E−01
^{38}Ar	9.8 E−04	1.2 E−01
^{40}Ar	1.3 E−09	1.2 E−05
^{39}K	7.2 E−05	4.3 E−02
^{41}K	6.9 E−06	5.3 E−02
^{40}Ca	4.1 E−02	1.3 E 00
^{42}Ca	2.2 E−05	9.9 E−02
^{43}Ca	1.7 E−08	3.2 E−04
^{44}Ca	8.2 E−05	1.1 E−01
^{46}Ca	6.9 E−12	5.5 E−06
^{48}Ca	2.2 E−13	3.0 E−09
^{45}Sc	5.7 E−07	3.1 E−02
^{46}Ti	4.8 E−05	4.1 E−01
^{47}Ti	9.9 E−07	9.1 E−03
^{48}Ti	3.1 E−06	2.7 E−03
^{49}Ti	1.6 E−05	1.8 E−01
^{50}Ti	1.1 E−06	1.3 E−02
^{50}V	8.4 E−09	2.1 E−02
^{51}V	2.6 E−05	1.5 E−01
^{50}Cr	3.3 E−04	9.1 E−01
^{52}Cr	7.7 E−03	1.1 E 00
^{53}Cr	2.8 E−03	3.3 E 00
^{54}Cr	3.0 E−05	1.4 E−01
^{55}Mn	8.0 E−03	1.2 E 00
^{54}Fe	1.5 E−01	3.9 E 00
^{56}Fe	6.1 E−01	1.0 E 00
^{57}Fe	1.1 E−02	7.5 E−01
^{58}Fe	2.1 E−04	9.3 E−02
^{59}Co	4.7 E−04	2.7 E−01
^{58}Ni	6.1 E−02	2.4 E 00
^{60}Ni	1.1 E−02	1.1 E 00
^{61}Ni	6.4 E−06	1.4 E−02
^{62}Ni	2.7 E−04	1.9 E−01
^{64}Ni	2.3 E−07	5.3 E−04
^{63}Cu	4.3 E−07	1.4 E−03
^{65}Cu	1.1 E−08	7.3 E−05

[a] $\langle X_i/^{56}\mathrm{Fe}\rangle \equiv [X_i/X(^{56}\mathrm{Fe})]/[X_i/X(^{56}\mathrm{Fe})]_\odot$.

TABLE 5

NUCLEOSYNTHESIS PRODUCTS FOR THE MODEL C6

Species	Mass ($M_\odot$)	$\langle X_i/X_i(^{56}\mathrm{Fe})\rangle$[a]
^{12}C	1.7 E−01	1.2 E−01
^{13}C	9.4 E−14	5.6 E−12
^{14}N	5.2 E−10	1.5 E−09
^{15}N	2.1 E−09	1.5 E−06
^{16}O	2.6 E−01	8.2 E−02
^{17}O	9.6 E−12	7.8 E−09
^{18}O	2.4 E−13	3.4 E−11
^{19}F	6.7 E−14	4.3 E−10
^{20}Ne	1.1 E−03	2.2 E−03
^{21}Ne	5.3 E−09	3.4 E−06
^{22}Ne	8.3 E−03	1.3 E−01
^{23}Na	1.3 E−06	8.8 E−05
^{24}Mg	1.7 E−02	8.1 E−02
^{25}Mg	4.5 E−06	1.6 E−04
^{26}Mg	3.0 E−06	9.3 E−05
^{27}Al	4.3 E−04	1.8 E−02
^{28}Si	1.3 E−01	4.8 E−01
^{29}Si	3.1 E−04	2.2 E−02
^{30}Si	3.3 E−03	3.4 E−01
^{31}P	1.4 E−04	6.7 E−02
^{32}S	6.8 E−02	4.2 E−01
^{33}S	5.8 E−04	4.4 E−01
^{34}S	1.5 E−03	1.9 E−01
^{36}S	2.1 E−08	8.0 E−04
^{35}Cl	7.8 E−05	5.9 E−02
^{37}Cl	1.9 E−05	4.2 E−02
^{36}Ar	1.8 E−02	5.4 E−01
^{38}Ar	7.2 E−04	1.1 E−01
^{40}Ar	8.6 E−10	1.0 E−05
^{39}K	4.9 E−05	3.7 E−02
^{41}K	4.9 E−06	4.7 E−02
^{40}Ca	3.5 E−02	1.4 E 00
^{42}Ca	1.5 E−04	8.8 E−02
^{43}Ca	1.0 E−08	2.5 E−04
^{44}Ca	6.3 E−05	1.1 E−01
^{46}Ca	2.4 E−12	2.4 E−06
^{48}Ca	0.0 E 00	0.0 E 00
^{45}Sc	4.3 E−07	2.9 E−02
^{46}Ti	3.5 E−05	3.8 E−01
^{47}Ti	7.3 E−07	8.4 E−03
^{48}Ti	2.0 E−06	2.2 E−03
^{49}Ti	1.1 E−05	1.7 E−01
^{50}Ti	1.3 E−10	2.0 E−06
^{50}V	3.5 E−09	1.1 E−02
^{51}V	1.7 E−05	1.2 E−01
^{50}Cr	2.4 E−04	8.5 E−01
^{52}Cr	5.4 E−03	9.3 E−01
^{53}Cr	2.1 E−03	3.1 E 00
^{54}Cr	2.4 E−07	1.4 E−03
^{55}Mn	5.6 E−03	1.0 E 00
^{54}Fe	1.1 E−01	3.6 E 00
^{56}Fe	4.9 E−01	1.0 E 00
^{57}Fe	7.9 E−03	6.7 E−01
^{58}Fe	5.8 E−07	3.2 E−04
^{59}Co	2.3 E−04	1.7 E−01
^{58}Ni	4.0 E−02	2.0 E 00
^{60}Ni	3.9 E−03	4.9 E−01
^{61}Ni	1.1 E−06	3.0 E−03
^{62}Ni	3.3 E−06	2.9 E−03
^{64}Ni	2.2 E−11	6.3 E−08
^{63}Cu	1.0 E−07	4.1 E−04
^{65}Cu	9.3 E−12	8.1 E−08

[a] $\langle X_i/^{56}\mathrm{Fe}\rangle \equiv [X_i/X(^{56}\mathrm{Fe})]/[X_i/X(^{56}\mathrm{Fe})]_\odot$.

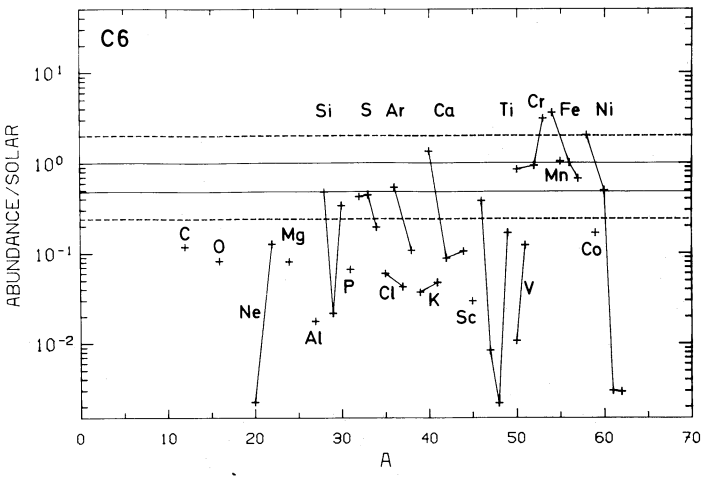

FIG. 11.—Same as Fig. 9 but for case C6

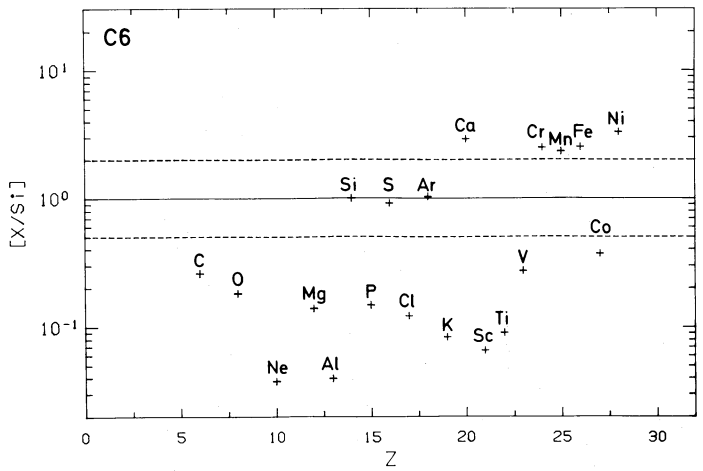

FIG. 12.—Same as Fig. 10 but for case C6

which is enough to power the light curve of SN I by the decays into Co and Fe.

The abundance ratios among the iron peak elements are generally in good agreement with the solar values as has been found for the carbon detonation models with similar central densities (Arnett, Truran, and Woosley 1971; Bruenn 1971). The exception is the ratio $^{54}Fe/^{56}Fe$ which is enhanced by a factor of 3.9 (W7) and 3.6 (C6) relative to the solar value. As discussed by Nomoto, Thielemann, and Wheeler (1984), such large enhancement of neutronization compared with the carbon detonation models may be due mainly to the significantly slower propagation of the deflagration wave than the detonation wave and also due to the enhanced electron capture rates (Fuller, Fowler, and Newman 1982) compared with the previous rates (Mazurek, Truran, and Cameron 1974).

The ratio $^{54}Fe/^{56}Fe$ depends on the distribution of the neutron excess, $\eta = 1 - 2Y_e$, in the NSE layer, which, in turn, depends on the ignition density and on the competitive processes of electron captures and the propagation of the deflagration wave: For lower $\rho_{c,ig}$ and faster deflagration wave, η is smaller in the central region. Therefore, the distribution of η or Y_e is sensitive to the treatment of the deflagration wave. In view of the uncertainties involved in the theory of convection, the overabundances of ^{54}Fe may not be so severe.

Dependence of the $^{54}Fe/^{56}Fe$ ratio on the electron capture rates for the NSE composition will be discussed in Thielemann, Nomoto, and Yokoi (1984); if the capture rates by Mazurek *et al.* (1974) are employed, the total rate is smaller by a factor of ~ 2 and the $^{54}Fe/^{56}Fe$ ratio is significantly reduced (see also Bruenn 1971).

Overproduction of ^{54}Cr and ^{55}Mn found in the earlier model reported in Nomoto (1984*b*) does not appear in the present model. In the earlier model, the NSE table was applied for $M_r < 0.7\ M_\odot$ instead of a full reaction network calculation which was done in the present study. The abundance of ^{53}Cr will be discussed in Thielemann, Nomoto, and Yokoi (1984).

To initiate a carbon deflagration at lower ρ_c than C6 would require an accretion as rapid as $\dot{M} \gtrsim 10^{-6}\ M_\odot\ \mathrm{yr}^{-1}$ which may occur in the double white dwarf scenario for SN I progenitors. However, it must be noted that the rapid accretion does not necessarily lead to the lower ignition density (Nomoto 1984*c*).

b) Intermediate-Mass Elements: Si-Ca

The abundances of Si-Ca are important for comparison with the early time spectra of SN I (Branch 1984*a*). Both models (W7 and C6) eject ^{40}Ca with the abundance ratio of $\langle ^{40}Ca/^{56}Fe\rangle \sim 1$, and ^{28}Si, ^{32}S, and ^{36}Ar with the ratio of $\langle X_i/^{56}Fe\rangle = 0.4$–$0.5$. Moreover, the relative abundance of ^{28}Si, ^{32}S, and ^{36}Ar are remarkably close to the solar values (Table 3). On the other hand, the abundances of odd-Z elements in Si-Ti range, i.e., P, Cl, K, and Sc, are as small as $\langle X_i/^{56}Fe\rangle = 0.03$–$0.07$.

It is noteworthy that Si peak elements are synthesized in the layer with relatively high density, i.e., $\rho_{p,7} = 2.5$–4. This is significantly higher than the 10^5–10^6 g cm^{-3} in the oxygen-rich layer of a 25 $M_\odot$ star where Si peak elements are produced (Woosley and Weaver 1982). Such a difference may cause the difference in the abundance patterns among Si peak elements.

c) s- and r-Process Elements

The carbon deflagration supernova is a possible source of *s*- and *r*-process elements. During the accretion onto the white dwarf, helium flashes recur many times when enough helium is accumulated below the hydrogen-burning shell. As demonstrated by Sugimoto *et al.* (1977), the helium shell flash develops a convective zone which mixes hydrogen into the helium layer. Subsequent reactions of $^{12}C(p, \gamma)^{13}N(e^+\nu)^{13}C(\alpha, n)^{16}O$ could produce neutrons to synthesize *s*-process elements. Even without such a mixing of hydrogen, the peak temperature during the helium shell flashes is high enough to produce neutrons via the $^{22}Ne(\alpha, n)^{25}Mg$ reaction for $M \gtrsim 1\ M_\odot$ (Iben 1975, 1981; Sugimoto and Nomoto 1975). Therefore, if hydrogen or helium accretes onto the white dwarf, the outer layer of the white dwarf contains some *s*-process elements at the explosion.

The carbon deflagration wave produces a precursor shock wave as discussed in § IV*b*. When the deflagration wave approaches at the white dwarf surface, the precursor shock grows strong because of the steep density gradient. If the temperature at the passage of the shock wave becomes high enough for the $^{22}Ne(\alpha, n)^{25}Mg$ reaction to generate neutrons, the *r*-process could operate on the seed *s*-process elements (Truran, Cowan, and Cameron 1978; Thielemann, Arnould, and Hillebrandt 1979; Cowan, Cameron, and Truran 1980). The amount of *s*- and *r*-process elements produced by this mechanism deserves further quantitative investigation.

TABLE 6

γ-RADIOACTIVITIES FROM CARBON DEFLAGRATION SUPERNOVAE

Species	W7[a]	C6[a]
^{22}Na	1.6 E−07	2.2 E−08
^{26}Al	3.8 E−06	3.8 E−07
^{44}Ti	8.2 E−05	6.3 E−05
^{48}V	2.7 E−07	2.0 E−07
^{56}Ni	5.8 E−01	4.8 E−01
^{56}Co	2.8 E−04	2.0 E−04
^{57}Co	2.5 E−03	1.3 E−03
^{60}Co	2.2 E−08	2.2 E−11
^{60}Fe	2.3 E−09	3.1 E−15

[a] Mass ($M_\odot$).

It should be noted that these *s*- and *r*-processes do not operate for the CO-CO double white dwarf system since no helium layer is formed.

d) Gamma-Radioactivities

Besides ^{56}Ni and ^{56}Co, SN I produces some γ-radioactivities, i.e., ^{22}Na, ^{26}Al, ^{44}Ti, ^{48}V, ^{57}Co, ^{60}Co, and ^{60}Fe as summarized in Table 6. The ^{26}Al/^{27}Al ratio is 6×10^{-3} (W7) and 9×10^{-4} (C6) which are larger than 5×10^{-4} in the 25 $M_\odot$ model (Woosley and Weaver 1982).

VII. CONTRIBUTION OF TYPE I SUPERNOVAE TO GALACTIC NUCLEOSYNTHESIS

If we adopt a carbon deflagration supernova model like case W7 as a typical SN I model, SN I make a significant contribution to the galactic nucleosynthesis in the Si-Ni range.

It has been pointed out that the intermediate mass elements, Si-Ca, are underproduced relative to ^{16}O in the ejecta of a 25 $M_\odot$ star which may be a typical site of massive star nucleosynthesis (Woosley and Weaver 1982). Woosley and Weaver (1982) proposed that elements in the range of S-Ti could be produced by stars more massive than 25 $M_\odot$ or very massive Population III stars. Arnett and Thielemann (1984) showed that a part of these problems can be removed with an enhanced ^{12}C(α, γ)^{16}O rate in He-burning.

Nomoto, Thielemann, and Wheeler (1984) investigated the importance of SN I to galactic nucleosynthesis. They summed up nucleosynthesis products from the W7 model (SN I) and the 25 $M_\odot$ model assuming that the 25 $M_\odot$ star is a typical Type II supernova regarding nucleosynthesis yields and that the explosion rate of SN II is equal to that for SN I. This combination shows an improved fit to the solar abundance ratios over a wide range in mass number A; i.e., SN I products tend to fill in a variety of isotopes in the gap of Si-Ni existing in the present SN II models. This suggests that a significant fraction of Si-Ca originate from SN I and that nucleosynthesis in the deflagration model for SN I is quite complementary to the SN II.

The absolute production rates of elements give some constraints on the SN rate. Nomoto, Thielemann, and Wheeler (1984) discussed this problem by comparing the Fe production rate from SN I with the observed rate in the solar neighborhood. Here we follow Tinsley (1980) and make a crude estimate of the abundance of the element, X_i, ejected from SN I by the yield $X_i \equiv m_i r/s$; here m_i is the mass of species i ejected by each SN I, r is the SN I rate, and s is the net star formation rate as discussed by Tinsley (1980). If we adopt values of $s = 5\ M_\odot$ pc^{-2} Gyr^{-1} (Tinsley 1980; see Yokoi, Takahashi, and Arnould 1983 for discussion on s) and $r = (0.01\text{–}0.03)$ pc^{-2} Gyr^{-1} (Tammann 1982), $X_i = (0.002\text{–}0.006)\,(m_i/M_\odot)$. Model W7 gives $X(^{56}\text{Fe}) = 0.0012\text{–}0.0037$ which is marginally consistent with the solar abundance if we adopt the lower limit for the SN I rate. If the SN I rate is higher, a part of the Fe from SN I may form grains or escape from the Galaxy.

Assuming $r = 0.01$ pc^{-2} Gyr^{-1} which corresponds to 10^{-2} yr^{-1} for the Galaxy (Tammann 1982), model W7 gives $\langle X(^{56}\text{Fe})\rangle \sim 0.92$, $\langle X(^{40}\text{Ca})\rangle \sim 1.1$, $\langle X(^{36}\text{Ar})\rangle \sim 0.47$, $\langle X(^{32}\text{S})\rangle \sim 0.37$, $\langle X(^{28}\text{Si})\rangle \sim 0.41$, $\langle X(^{24}\text{Mg})\rangle \sim 0.080$, $\langle X(^{16}\text{O})\rangle \sim 0.033$, and $\langle X(^{12}\text{C})\rangle \sim 0.016$, where $\langle\ \rangle$ denotes the abundance ratio with respect to the solar values. Therefore SN I could also produce a significant fraction of ^{40}Ca and Si peak elements in the Galaxy besides iron peak elements.

VIII. COMPARISON WITH OBSERVATIONS

a) Light Curves

The carbon deflagration supernova models presented here eject 0.5–0.7 $M_\odot$ ^{56}Ni. The approximate light curves powered by the radioactive decays of ^{56}Ni and ^{56}Co were calculated for the present models of W7 and C6 by adopting the approximation by Chevalier (1981). The bolometric luminosity is shown in Figure 13 where optical opacity is assumed to be $\kappa = 0.1$ cm^2 g^{-1}. Detailed comparison with observations is beyond our present scope, since a UV deficiency in the spectrum should be taken into account to obtain the blue magnitude (Branch *et al.* 1983). (See Schurmann 1983 and Sutherland and Wheeler 1984 for such a calculation.) However, qualitative characteristics of the SN I light curves are well reproduced in Figure 13 as discussed by Chevalier (1981) and Arnett (1982) for similar models.

The peak bolometric luminosities are 1.3×10^{43} ergs s^{-1} for case W7 and 1.0×10^{43} ergs s^{-1} for case C6 and consistent with the observed value of 2×10^{43} ergs s^{-1} $(H_0/50$ km s^{-1} Mpc$^{-1})^{-2}$ (Wheeler, Branch, and Falk 1980) within the uncertainties involved in κ and H_0.

Sutherland and Wheeler (1984) argued that at least 0.7 $M_\odot$ ^{56}Ni must be produced to give a proper rise time and the photospheric expansion velocity at maximum light (see also Branch 1984*a*). In the present models, significant fraction of the explosion energy originates from the production of non–^{56}Ni elements (neutron-rich isotopes and intermediate mass

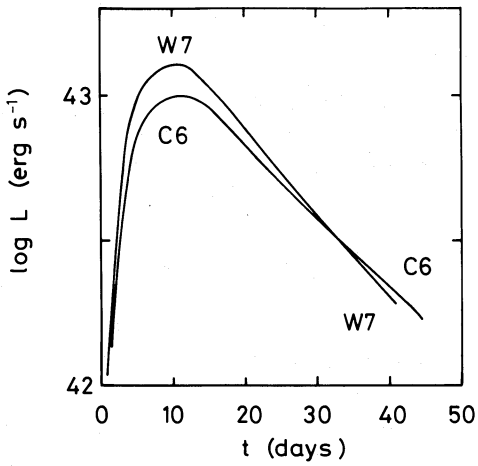

FIG. 13.—Approximate light curves due to readioactive decays of ^{56}Ni and ^{56}Co for cases W7 and C6. Bolometric luminosities are shown. These curves are calculated based on the approximation by Chevalier (1981) assuming optical opacity of 0.1 cm^2 g^{-1}.

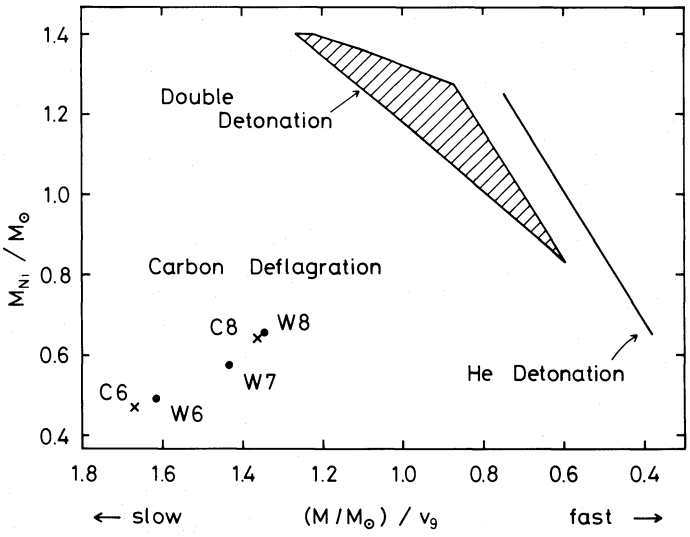

FIG. 14.—The brightness ($\propto M_{Ni}$) and the speed class (indicated by M/v) of the light curves due to radioactive decays, where $v_9 \equiv v/(10^9$ cm s$^{-1})$ is the velocity scale (Arnett 1982). Possible ranges for various types of explosion are indicated, i.e., He detonation in He white dwarfs, double detonations in C + O white dwarfs, and several carbon deflagration models in the present study.

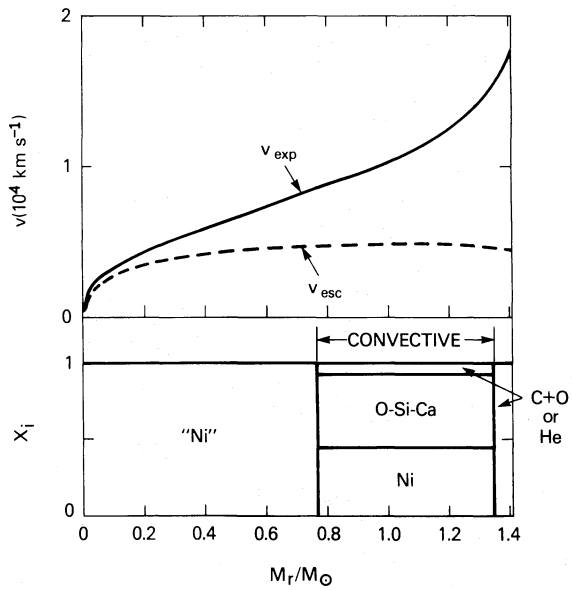

FIG. 15.—Composition structure and the velocity profile of the carbon deflagration model by Nomoto (1980*a*) where the convectively unstable layers behind the deflagration wave are mixed.

elements). Therefore, even for case C6 which produces only 0.5 $M_\odot$ ^{56}Ni, the rise time and the expansion velocity in the outer layers (see § IV*c*) may be consistent with the observations.

Figure 14 shows a ($M_{Ni} - M/v$) plane which characterizes the brightness and the shape of light curves: the mass of ^{56}Ni, M_{Ni}, is approximately proportional to the maximum luminosity. The ratio M/v is related to the width (or speed class) of the light curves since the effective diffusion time is given by $\tau_m \equiv (\kappa M/v)^{1/2}$ (Arnett 1982), where M is the total ejected mass and $v \propto (E/M)^{1/2}$ is the velocity scale. Compared with the detonation type models in Figure 14, the light curves of the deflagration models are dimmer and broader, i.e., they decline more slowly.

For the models with the same α but different $\dot{M}$, e.g., C6-W6 or C8-W8 pair, their locations in Figure 14 are very close to each other. This is due mainly to the fact that the carbon ignition density is not sensitive to $\dot{M}$. This may be consistent with the uniformity of SN I. However, Pskovskii (1977) and Branch (1981) suggested the existence of such a variation among SN I light curves that the brighter one shows slower decline. The carbon deflagration models show an opposite tendency, though small. On the other hand, the detonation models show a brighter-slower tendency as seen in Figure 14. Whether this is a serious trouble for the deflagration model may need further study on both the observational and the theoretical sides.

b) Early Time Spectra

The early time spectra of SN I show the composition structure in the outer layer which is expanding at $\sim 10^4$ km s^{-1} (Branch 1984*a*). The synthetic spectra for the model W7 has recently been calculated (Branch 1984*b*). A fit to the observed spectra of SN I 1981*b* at maximum light and 17 days later is fairly good provided that the outer layers at $M_r \gtrsim 0.7\ M_\odot$ are mixed. On the other hand, the spectra for the models with complete composition stratification do not show a good fit.

Although a mixing process after passage of the deflagration wave was not included in the present calculation, convective mixing in the outer layers is expected to occur because of the decaying nature of the deflagration wave: The incinerated NSE region is almost isothermal and thus convectively stable. On the other hand, material in the outer layers at $M_r \gtrsim 0.7\ M_\odot$ is processed by the decaying deflagration wave and the nuclear energy release gets smaller as the deflagration wave decays. Therefore, such layers are convectively unstable because of outward decrease in entropy which leads to even a density inversion.

Such a mixing behind the deflagration wave was taken into account in the model by Nomoto (1980*a*) where the convectively unstable layers were assumed to mix quickly. The resultant composition and velocity profile are shown in Figure 15. Since the evolutionary time scale is rather short, however, the actual mixing may not be complete. More accurate calculation should be done to obtain the real composition structure. It also needs to be studied that to what extent the composition stratification must be erased to get a reasonable fit between the observed and synthetic spectra.

c) Remnant

The carbon deflagration model predicts complete disruption of the star leaving no neutron star remnant behind. This is consistent with the failure to detect point X-ray sources or X-ray nebulae in the SN I remnants (Helfand and Becker 1984) and the latest model of neutron star cooling (Nomoto and Tsuruta 1981).

The present model is also consistent with the *IUE* observations of the remnant of SN 1006 and X-ray observations of SN I remnants which suggest the existence of some Si peak elements in the outer layers of the ejecta.

IX. CONCLUSIONS AND DISCUSSION

a) Carbon Deflagration Models

We have shown that many of the observed features of SN I, in particular near maximum light, can be accounted for by the carbon deflagration model in accreting white dwarfs. Main

features of this model based on the detailed nucleosynthesis calculation are as follows:

1. The carbon deflagration is initiated by the relatively rapid accretion. During the accretion, the interior of the white dwarf is heated up, and thus the carbon ignition condition does not depend much on the initial state of the white dwarf.

2. The carbon deflagration wave synthesizes $\sim 0.6\ M_\odot$ ^{56}Ni in the inner layers. This amount of ^{56}Ni is sufficient to power the SN I light curve by the radioactive decays into ^{56}Co and ^{56}Fe.

3. In the outer layers of the white dwarf, substantial amount of intermediated mass elements such as Ca, Ar, S, Si, Mg, and O are synthesized. The synthetic spectra based on this model shows a good fit to the early time spectra of SN I provided that the outer layers are mixed (Branch 1984*b*).

4. SN I may produce significant fraction of Ca-Si in the Galaxy besides iron peak elements. Such nucleosynthesis in SN I may be complementary to the nuclear products from massive stars.

It must be remembered that carbon deflagration models include a highly uncertain parameter (i.e., $\alpha = l/H_p$) for the propagation speed of the deflagration wave and the outcome is rather sensitive to α (see also Sutherland and Wheeler 1984; Woosley, Axelrod, and Weaver 1984). The above calculation is based on the appropriate choice of α which yields reasonable explosion energy ($\sim 10^{51}$ ergs s^{-1}). For smaller α, explosion energy may be too small (see the model with the explosion energy of 5×10^{49} ergs calculated by Nomoto, Sugimoto, and Neo 1976), while a model with $\alpha = 1$ was found to produce almost exclusively iron peak elements according to our preliminary calculation. Both may be incompatible with SN I observations.

It should also be noted that the present models undergo excess neutronization in the central region and yield excess ^{54}Fe relative to ^{56}Fe by a factor of ~ 4. This may be related to the uncertainties in the rapidity of deflagration wave or might impose restriction on the central ignition density.

It needs to be studied whether the deflagration model starting from the lower $\rho_{c,ig}$ (i.e., higher $\dot{M}$) is consistent with the SN I observations; in particular, effects of a possible difference in the initial composition of the white dwarf might be significant (see the next section).

b) *Progenitor Stars*

Evolutionary calculations of accreting white dwarfs predict the occurrence of a different type of explosion for the slow accretion, namely, detonation supernovae triggered by a helium flash (§ I). However, the detonation-type explosion produces almost exclusively iron peak elements, which is inconsistent with the observations (Paper II).

Then the question is why the carbon deflagration occurs much more frequently in nature than the detonation-type supernova (Branch 1984*a*). Possible answers may be one or more of the following:

1. For C + O white dwarfs, the carbon deflagration is simply more frequent than the double detonations because the deflagration occurs for more rapid accretion (see Fig. 1).

2. The occurrence of a detonation-type explosion is rare because hydrogen shell flashes for the slow accretion are so strong that most of the accreted matter is lost from the white dwarf and cannot build up a helium layer with sufficient mass.

3. Most of SN I originate from the double white dwarf systems (Iben and Tutukov 1984; Webbink 1984). In this case, the accretion rate is so high that the double detonation supernova corresponding to slow $\dot{M}$ must be a rare event. Only the C + O white dwarf pair could become SN I and the He white dwarf pair may not explode for some reason, e.g., too small a total mass.

It must be noted that the evolution of the white dwarf undergoing such a rapid accretion as $\dot{M} > \dot{M}_{\rm AGB}$ may be quite different from the models with $\dot{M} < \dot{M}_{\rm AGB}$ considered here. First, the carbon flash is ignited in the outer shell, and the burning shell moves inward (Nomoto 1982*c*). Whether or not the burning shell reaches the center to yield O + Ne + Mg white dwarfs needs more investigation. Second, the ignition density depends on the initial temperature of the white dwarf because the accretion time scale is too short for conduction to heat up the center. Therefore the ultimate fate of this class of white dwarfs could be significantly different from the present models.

c) *Collapse of White Dwarfs in Silent Supernovae*

The thermonuclear explosion disrupts the white dwarf completely leaving no neutron star remnant behind except for the case with a single detonation leaving a white dwarf remnant. On the other hand, the evolutionary origin of low-mass X-ray binary systems and a binary containing the 6.1 ms pulsar might be a collapse of a certain class of accreting white dwarfs to form neutron stars (e.g., van den Heuvel 1981; Helfand, Ruderman, and Shaham 1983). Therefore it is interesting to explore the possibility of white dwarf collapse and its relation to SN I.

In this regard, possible effects of carbon and oxygen separation in the crystallizing white dwarf have been investigated by Isern *et al.* (1983) and Mochkovich (1983) although such a separation is quite hypothetical (S. Ichimaru 1983, private communication). If the separation occurs, a solid oxygen core is formed interior to the C + O layers. The probable outcome of the accretion onto such a white dwarf may be the off-center carbon ignition prior to the onset of electron captures on ^{16}O at the center. Therefore the outcome could be SN I rather than collapse to form neutron stars.

However, collapse of accreting white dwarfs can occur for O + Ne + Mg white dwarfs because electron captures on ^{24}Mg and ^{20}Ne trigger the collapse prior to the explosion (Nomoto *et al.* 1979; Miyaji *et al.* 1980). Such O + Ne + Mg white dwarfs form from 8–10 $M_\odot$ stars in close binary systems (Nomoto 1980*a*, 1984*a*). Although the frequency of collapse is several orders of magnitude smaller than SN I, it may be consistent with the statistics of low-mass X-ray binaries and binary pulsars (van den Heuvel 1981; Webbink, Rappaport, and Savonije 1983; Iben and Tutukov 1984). The collapsing white dwarf will make a bounce and eject a small amount of material as found in 8–10 $M_\odot$ stars (Hillebrandt, Nomoto, and Wolff 1984). Because of the lack of either ^{56}Ni or an extended envelope, however, the explosion would be *silent*.

We would like to thank Drs. D. Branch and J. C. Wheeler for useful discussion on the synthetic spectra and galactic nucleosynthesis. K. N. is indebted to Drs. R. Kippenhahn, W. Hillebrandt, E. Müller, I. Iben, and J. W. Truran for stimulating discussion and hospitality during the stay at the Max-Planck-Institut and the University of Illinois, and to Professors D. Sugimoto and S. Ichimaru for useful discussion and comments. This work is supported in part by the Japanese Ministry of Education, Science, and Culture through Research Grant No. 58340023 and by the Space Data Analysis Center, Institute of Space and Astronautical Sciences, Tokyo.

REFERENCES

Arnett, W. D. 1969, *Ap. Space Sci.*, **5**, 180.
———. 1979, *Ap. J. (Letters)*, **230**, L37.
———. 1982, *Ap. J.*, **253**, 785.
Arnett, W. D., and Thielemann, F.-K. 1984, in *Stellar Nucleosynthesis*, ed. C. Chiosi and A. Renzini (Dordrecht: Reidel), p. 145.
Arnett, W. D., Truran, J. W., and Woosley, S. E., 1971, *Ap. J.*, **165**, 87.
Axelrod, T. S. 1980*a* in *Type I Supernovae*, ed. J. C. Wheeler (Austin: University of Texas), p. 80.
———. 1980*b*, Ph.D. thesis, University of California at Santa Cruz.
Becker, R. H., Holt, S. S., Smith, B. W., White, N. E., Boldt, E. A., Mushotzky, R. F., and Serlemitos, P. J. 1980, *Ap. J. (Letters)*, **235**, L5.
Branch, D. 1981, *Ap. J.*, **248**, 1076.
———. 1984*a*, in *Ann. NY Acad. Sci.*, **422**, 186.
———. 1984*b*, in *Proc. Workshop on Challenges and New Developments in Nucleosynthesis* (Chicago: University of Chicago Press), in press.
Branch, D., Buta, R., Falk, S. W., McCall, M. L., Sutherland, P. G., Uomoto, A., Wheeler, J. C., and Wills, B. J. 1982, *Ap. J. (Letters)*, **252**, L61.
Branch, D., Lacy, C. H., McCall, M. L., Sutherland, P. G., Uomoto, A., Wheeler, J. C., and Wills, B. J. 1983, *Ap. J.*, **270**, 123.
Bruenn, S. W. 1971, *Ap. J.*, **168**, 203.
Buchler, J. R., and Mazurek, T. J. 1975, *Mem. Soc. Roy. Sci. Liège*, **8**, 435.
Cameron, A. G. W. 1982, in *Essays in Nuclear Astrophysics*, ed. C. A. Barnes, D. D. Clayton, and D. N. Schramm, (Cambridge: Cambridge University Press), p. 23.
Chevalier, R. A. 1981, *Ap. J.*, **246**, 267.
Colgate, S. A., Petschek, A. G., and Kriese, J. T. 1980, *Ap. J. (Letters)*, **237**, L81.
Courant, R., and Friedrichs, K. O. 1948, *Supersonic Flow and Shock Waves* (New York: Interscience).
Cowan, J. J., Cameron, A. G. W., and Truran, J. W. 1980, *Ap. J.*, **241**, 1090.
Ergma, E. V., and Tutukov, A. V. 1976, *Acta Astr.*, **26**, 69.
Fowler, W. A. 1981, private communication.
Fowler, W. A., Caughlan, G. R., and Zimmerman, B. A. 1975, *Ann. Rev. Astr. Ap.*, **13**, 69.
Fujimoto, M. Y., and Sugimoto, D. 1982, *Ap. J.*, **257**, 291.
Fuller, G. M., Fowler, W. A., and Newman, M. 1980, *Ap. J. Suppl.*, **42**, 447.
———. 1982, *Ap. J. Suppl.*, **48**, 279.
Hansen, C. J., and Wheeler, J. C. 1969, *Ap. Space Sci.*, **36**, 464.
Hayashi, C., Hōshi, R., and Sugimoto, D. 1962, *Progr. Theoret. Phys. Suppl.*, **22**, 1.
Helfand, D. J., and Becker, R. H. 1984, *Nature*, **307**, 215.
Helfand, D. J., Ruderman, M. A., and Shaham, J. 1983, *Nature*, **304**, 423.
Hillebrandt, W., Nomoto, K., and Wolff, R. G. 1984, *Astr. Ap.*, **133**, 175.
Hoyle, F., and Fowler, W. A. 1960, *Ap. J.*, **132**, 565.
Iben, I., Jr. 1975, *Ap. J.*, **196**, 525.
———. 1981, *Ap. J.*, **243**, 987.
———. 1982, *Ap. J.*, **259**, 244.
Iben, I., Jr., and Tutukov, A. V. 1984, *Ap. J. Suppl.*, **55**, 335.
Ichimaru, S. 1982, *Rev. Mod. Phys.*, **54**, 1017.
Ichimaru, S., and Utsumi, K. 1983, *Ap. J. (Letters)*, **269**, L51.
———. 1984, *Ap. J.*, **278**, 382.
Isern, J., Labay, J., Hernanz, M., and Canal, R. 1983, *Ap. J.*, **273**, 320.
Itoh, N., and Kohyama, Y. 1983, *Ap. J.*, **275**, 858.
Itoh, N., Mitake, S., Iyetomi, H., and Ichimaru, S. 1983, *Ap. J.*, **273**, 774.
Ivanova, L. N., Imshennik, V. S., and Chechetkin, V. M. 1974, *Ap. Space Sci.*, **31**, 497.
Mazurek, T. J., Cooperstein, J., and Kahana, S. 1980, in *DUMAND-80*, ed. V. J. Stenger, (Honolulu: Hawaii-DUMAND center), p. 142.
Mazurek, T. J., Meier, D. L., and Wheeler, J. C. 1977, *Ap. J.*, **213**, 518.
Mazurek, T. J., Truran, J. W., and Cameron, A. G. W. 1974, *Ap. Space Sci.*, **27**, 261.
Meyerott, R. E. 1980, *Ap. J.*, **239**, 257.
Miyaji, S., Nomoto, K., Yokoi, K., and Sugimoto, D. 1980, *Pub. Astr. Soc. Japan*, **32**, 303.
Mochkovitch, R. 1983, *Astr. Ap.*, **122**, 212.
Müller, E., and Arnett, W. D. 1982, *Ap. J. (Letters)*, **261**, L107.
———. 1984, *Ap. J.*, submitted.
Nomoto, K. 1980*a*, in *Type I Supernovae*, ed. J. C. Wheeler (Austin: University of Texas), p. 164.
———. 1980*b*, *Space Sci. Rev.*, **27**, 563.
———. 1981, in *IAU Symposium 93, Fundamental Problems in the Theory of Stellar Evolution*, ed. D. Sugimoto, D. Q. Lamb, and D. N. Schramm (Dordrecht: Reidel), p. 295.
Nomoto, K. 1982*a*, *Ap. J.*, **253**, 798 (Paper I).
———. 1982*b*, *Ap. J.*, **257**, 780 (Paper II).
———. 1982*c*, in *Supernovae: A Survey of Current Research*, ed. M. J. Rees and R. J. Stoneham (Dordrecht: Reidel), p. 205.
———. 1984*a*, *Ap. J.*, **277**, 791.
———. 1984*b*, in *Stellar Nucleosynthesis*, ed. C. Chiosi and A. Renzini (Dordrecht: Reidel), p. 205 and p. 238.
———. 1984*c*, in *Proc. Workshop on Challenges and New Developments in Nucleosynthesis* (Chicago: University of Chicago Press), in press.
Nomoto, K., Miyaji, S., Sugimoto, D., and Yokoi, K. 1979, in *IAU Colloquium 53, White Dwarfs and Variable Degenerate Stars*, ed. H. M. Van Horn and V. Weidemann (Rochester: University of Rochester), p. 56.
Nomoto, K., and Sugimoto, D. 1977, *Pub. Astr. Soc. Japan*, **29**, 765.
Nomoto, K., Sugimoto, D., and Neo, S. 1976, *Ap. Space Sci.*, **39**, L37.
Nomoto, K., Thielemann, F.-K., and Wheeler, J. C. 1984, *Ap. J. (Letters)*, **279**, L23; Erratum 1984, *Ap. J. (Letters)*, **283**, L25.
Nomoto, K., and Tsuruta, S. 1981, *Ap. J. (Letters)*, **250**, L19.
Ōno, Y. 1960, *Progr. Theoret. Phys.*, **24**, 825.
Pskovski, Y. P. 1977, *Sov. Astr.–AJ*, **21**, 675.
Shull, J. M. 1982, *Ap. J.*, **262**, 308.
Shurmann, S. R. 1983, *Ap. J.*, **267**, 779.
Slattery, W. L., Doolen, G. D., and DeWitt, H. E. 1982, *Phys. Rev. A.*, **26**, 2255.
Sugimoto, D., Fujimoto, M. Y., Nariai, K., and Nomoto, K. 1977, in *IAU Symposium 76, Planetary Nebulae*, ed. Y. Terzian (Dordrecht: Reidel), p. 208.
Sugimoto, D., and Nomoto, K. 1975, *Pub. Astr. Soc. Japan*, **27**, 197.
———. 1980, *Space Sci. Rev.*, **25**, 155.
Sugimoto, D., Nomoto, K., and Eriguchi, Y. 1982, *Prog. Theoret. Phys. Suppl.*, **70**, 115.
Sutherland, P., and Wheeler, J. C. 1984, *Ap. J.*, **280**, 282.
Taam, R. E. 1980, *Ap. J.*, **237**, 142.
Tammann, G. A. 1982, in *Supernovae: A Survey of Current Research*, ed. M. J. Rees and R. J. Stoneham (Dordrecht: Reidel), p. 371.
Thielemann, F.-K. 1980, Ph.D. thesis, TH Darmstadt and MPI Munich.
Thielemann, F.-K., Arnould, M., and Hillebrandt, W. 1979, *Astr. Ap.*, **74**, 175.
Thielemann, F.-K., Nomoto, K., and Yokoi, K. 1984, in preparation.
Tinsley, B. M. 1980, in *Type I Supernovae*, ed. J. C. Wheeler (Austin: University of Texas), p. 196.
Trimble, V. 1982, *Rev. Mod. Phys.*, **54**, 1183.
Truran, J. W., Cowan, J. J., and Cameron, A. G. W. 1978, *Ap. J. (Letters)*, **222**, L63.
Unno, W. 1967, *Pub. Astr. Soc. Japan*, **19**, 140.
van den Heuvel, E. P. J. 1981, in *IAU Sympsoum 93, Fundamental Problems in the Theory of Stellar Evolution*, ed. D. Sugimoto, D. Q. Lamb, and D. N. Schramm (Dordrecht: Reidel), p. 155.
Wagoner, R. V. 1969, *Ap. J. Suppl.*, **18**, 247.
Wagoner, R. V., Fowler, W. A., and Hoyle, F. 1967, *Ap. J.*, **148**, 3.
Wallace, R. K., and Woosley, S. E. 1981, *Ap. J. Suppl.*, **45**, 389.
Weaver, T. A., Axelrod, T. S., and Woosley, S. E. 1980, in *Type I Supernovae*, ed. J. C. Wheeler (Austin: University of Texas), p. 113.
Webbink, R. F. 1984, *Ap. J.*, **277**, 355.
Webbink, R. F., Rappaport, S., and Savonije, G. J. 1983, *Ap. J.*, **270**, 678.
Wheeler, J. C. 1982, in *Supernovae: A Survey of Current Research*, ed. M. J. Rees and R. J. Stoneham (Dordrecht: Reidel), p. 167.
Wheeler, J. C., Branch, D., and Falk, S. W., Jr. 1980, in *Type I Supernovae*, ed. J. C. Wheeler (Austin: University of Texas), p. 199.
Woosley, S. E., Axelrod, T. S., and Weaver, T. A. 1984, in *Stellar Nucleosynthesis*, ed. C. Chiosi and A. Renzini (Dordrecht: Reidel), p. 263.
Woosley, S. E., Fowler, W. A., Holms, J. A., and Zimmerman, B. A. 1975, Caltech preprint, OAP-422.
———. 1978, *Atomic Data and Nuclear Tables*, **22**, 371.
Woosley, S. E., and Weaver, T. A. 1982, in *Essays in Nuclear Astrophysics*, ed. C. A. Barnes, D. D. Clayton, and D. N. Schramm (Cambridge: Cambridge University Press), p. 377.
Woosley, S. E., Weaver, T. A., and Taam, R. E. 1980, in *Type I Supernovae*, ed. J. C. Wheeler (Austin: University of Texas), p. 96.
Wu, C.-C., Leventhal, M., Sarazin, C. L., and Gull, T. R. 1983, *Ap. J. (Letters)*, **269**, L5.
Yokoi, K., Neo, S., and Nomoto, K. 1979, *Astr. Ap.*, **77**, 210.
Yokoi, K., Takahashi, K., and Arnould, M. 1983, *Astr. Ap.*, **117**, 65.

KEN'ICHI NOMOTO: Department of Earth Science and Astronomy, College of Arts and Sciences, University of Tokyo, Meguro-ku, Tokyo 153, Japan

FRIEDRICH-K. THIELEMANN: Max-Planck-Institut für Physik und Astrophysik, Institut für Astrophysik, 8046 Garching bei München, West Germany

KOICHI YOKOI: Kernforschungszentrum Karlsruhe GmbH, Institut für Kernphysik III, D-7500 Karlsruhe, West Germany